

12

AFGL-TR-82-0264  
ENVIRONMENTAL RESEARCH PAPERS, NO. 733



ADA 124314

# Tides in the Thermosphere: A Review

J. M. FORBES  
K.S.W. CHAMPION

13 September 1982

DTIC  
FEB 10 1983  
H

Approved for public release; distribution unlimited.

DTIC FILE COPY

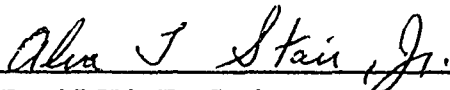
AERONOMY DIVISION PROJECT 6690  
AIR FORCE GEOPHYSICS LABORATORY  
HANSCOM AFB, MASSACHUSETTS 01731

AIR FORCE SYSTEMS COMMAND, USAF



This report has been reviewed by the ESD Public Affairs Office (PA)  
and is releasable to the National Technical Information Service (NTIS).

This technical report has been reviewed and  
is approved for publication.

  
\_\_\_\_\_  
DR. ALVA T. STAIR, Jr  
Chief Scientist

Qualified requestors may obtain additional copies from the  
Defense Technical Information Center. All others should apply  
to the National Technical Information Service.

Unclassified

SECURITY CLASSIFICATION OF THIS PAGE (When Data Entered)

REPORT DOCUMENTATION PAGE		READ INSTRUCTIONS BEFORE COMPLETING FORM
1. REPORT NUMBER AFGL-TR-82-0264	2. GOVT ACCESSION NO. AD-A124314	3. RECIPIENT'S CATALOG NUMBER 4
4. TITLE (and Subtitle) TIDES IN THE THERMOSPHERE: A REVIEW		5. TYPE OF REPORT & PERIOD COVERED Scientific. Interim.
		C. PERFORMING ORG. REPORT NUMBER ERP, No. 793
7. AUTHOR(s) J. M. Forbes* K. S. W. Champion		8. CONTRACT OR GRANT NUMBER(s)
9. PERFORMING ORGANIZATION NAME AND ADDRESS Air Force Geophysics Laboratory (LKB) Hanscom AFB Massachusetts 01731		10. PROGRAM ELEMENT, PROJECT, TASK AREA & WORK UNIT NUMBERS 62101F 66900709
11. CONTROLLING OFFICE NAME AND ADDRESS Air Force Geophysics Laboratory (LKB) Hanscom AFB Massachusetts 01731		12. REPORT DATE 13 September 1982
		13. NUMBER OF PAGES 42
14. MONITORING AGENCY NAME & ADDRESS (if different from Controlling Office)		15. SECURITY CLASS. (of this report) Unclassified
		15a. DECLASSIFICATION/DOWNGRADING SCHEDULE
16. DISTRIBUTION STATEMENT (of this Report)  Approved for public release; distribution unlimited.		
17. DISTRIBUTION STATEMENT (of the abstract entered in Block 20, if different from Report)		
18. SUPPLEMENTARY NOTES  *Dept. of Physics, Boston College, Chestnut Hill, MA 02167		
19. KEY WORDS (Continue on reverse side if necessary and identify by block number) Thermospheric tidal equations Thermospheric winds Thermospheric temperatures Semidiurnal thermospheric tide		
20. ABSTRACT (Continue on reverse side if necessary and identify by block number) A comprehensive review of recent theoretical and observational accomplishments relating to diurnal and semidiurnal tidal oscillations of neutral winds, temperature, density, and composition above 100 km is presented. Topics emphasized include: (1) Recent theoretical studies; (2) Solar cycle, seasonal, and latitudinal variations in tidal oscillations of temperature and winds as inferred from Thomson scatter measurements; (3) Tidal variations		

DD FORM 1473 1 JAN 73 EDITION OF 1 NOV 65 IS OBSOLETE

Unclassified

SECURITY CLASSIFICATION OF THIS PAGE (When Data Entered)

Unclassified

SECURITY CLASSIFICATION OF THIS PAGE(When Data Entered)

20. Abstract (Continued)

in total mass density and composition as inferred from satellite accelerometer and mass spectrometer measurements; (4) Comparison of recent theoretical models with the above observations; (5) The relative influence of in situ and propagating tides in determining the total semidiurnal thermospheric tide; and (6) Propagating tides of lower atmosphere origin as a source of mean momentum and heat in the lower thermosphere.

Unclassified

SECURITY CLASSIFICATION OF THIS PAGE(When Data Entered)

Accession For	
NTIS GRA&I	<input checked="" type="checkbox"/>
DTIC TAB	<input type="checkbox"/>
Unannounced	<input type="checkbox"/>
Justification	
By	
Distribution/	
Availability Codes	
Dist	Avail and/or Special
A	



## Contents

1. THEORETICAL STUDIES	7
2. TIDES FROM THOMSON SCATTER MEASUREMENTS	24
3. TIDES IN COMPOSITION AND TOTAL MASS DENSITY	28
4. ACCELERATION AND HEATING OF THE LOWER THERMOSPHERE DUE TO DISSIPATING TIDAL WAVES	36
REFERENCES	41

## Illustrations

1. Schematic Describing the Numerical Model of Atmospheric Tides Developed by Forbes <sup>1,2</sup>	8
2. Diurnal Heating Rates Due to UV and EUV Absorption in the Thermosphere (Forbes <sup>1,2</sup> )	9
3. Solar Diurnal Solstitial Westerly Winds From the Forbes <sup>1</sup> Model Corresponding to $T_o = 1000$ K	10
4. Northerly Velocity at $18^\circ$ Latitude Due to In Situ Excitation, the Propagating (1, 1) Mode and the Sum of These Sources	11
5. Diurnal Northerly Velocities at Arecibo ( $18^\circ$ N) (Harper <sup>5</sup> ) Compared With the Forbes <sup>1</sup> Model	11
6. Semidiurnal Heating Rates Due to UV and EUV Absorption in the Thermosphere (Forbes <sup>1,2</sup> )	12



## Illustrations

21. Example of Millstone Hill Neutral Exospheric Temperature Data During a Magnetically Quiet Day at Solar Minimum	25
22. Millstone Hill Diurnal Mean Temperatures vs $F_{10.7}$ and MSIS Model Prediction	26
23. Millstone Hill Diurnal Temperature Amplitudes vs $T_o$ (Hagan et al <sup>11</sup> )	27
24. Phase of Diurnal Temperature at Millstone Hill vs Day of Year Compared to MSIS Model (Hagan et al <sup>11</sup> )	28
25. Millstone Hill Semidiurnal Temperature Amplitudes vs $T_o$ (Hagan et al <sup>11</sup> )	29
26. Phase of Semidiurnal Temperature at Millstone Hill vs. Day of Year Compared to MSIS Model (Hagan et al <sup>11</sup> )	29
27. Plots of (Left) Amplitudes and (Right) Phase of Diurnal Variations in O (Crosses), O <sub>2</sub> (Circles), N <sub>2</sub> (Asterisks), Ar (Pluses), He (Triangles), and H (Double Triangles) at (Top) SSMIN and (Bottom) SSMAX at the Equator Under Equinox Conditions (From the Theoretical Model of Forbes <sup>16</sup> )	30
28. Diurnal Variations in O, N <sub>2</sub> and Total Mass Density Compared With AE-E Mass Spectrometer O ( $\Delta$ ) and N <sub>2</sub> (o), and Accelerometer Total Mass Density ( $\bullet$ ) Measurements (Forbes and Marcos <sup>18</sup> )	32
29. Diurnal Phase of Total Mass Density Compared With Phases Determined From Satellite Accelerometer Measurements (Forbes and Marcos <sup>18</sup> )	34
30. Atomic Oxygen Semidiurnal Variation (Hedin et al <sup>22</sup> )	35
31. Molecular Nitrogen Semidiurnal Variation (Hedin et al <sup>22</sup> )	35
32. Mean Zonal Wind ( $m\ sec^{-1}$ ) Due to Solar Heating Alone From Equinox Model of Dickinson et al <sup>23</sup>	37
33. Divergence of Eddy Momentum Flux ( $F_u$ ) and Zonal Mean Wind Due to (1, 1) Tidal Mode (Miyahara <sup>24</sup> )	38
34. Divergence of Eddy Momentum Flux ( $F_u$ ) and Zonal Mean Wind Due to (2, 4) Mode (Miyahara <sup>24</sup> )	39

## Tides in the Thermosphere: A Review

### 1. THEORETICAL STUDIES

Figure 1 illustrates schematically the various forcing mechanisms and physical processes that must be taken into account in order to comprehensively model tidal oscillations from the surface to the upper thermosphere (about 500 km), and basically describes a recent numerical model developed by Forbes.<sup>1,2</sup> He solves the linearized coupled momentum, continuity, and thermal energy equations for tidal perturbations in a viscous, rotating, spherical atmosphere from the surface to 400 km, taking into account realistic parameterization of background winds, temperature, composition, hydromagnetic coupling, Newtonian cooling, eddy and molecular diffusion, and tidal forcing mechanisms. Excitation of tidal oscillations in the model occurs via absorption of EUV and UV radiation in the thermosphere, H<sub>2</sub>O insolation absorption in the troposphere and lower stratosphere, O<sub>3</sub> insolation absorption in the mesosphere, ion-neutral momentum coupling in the F-region, and lunar gravitational forcing.

---

(Received for publication 10 September 1982)

1. Forbes, J. M. (1982) Atmospheric tides. I. Model description and results for the solar diurnal component, J. Geophys. Res. 87:5222-5240.
2. Forbes, J. M. (1982) Atmospheric tides. II. The solar and lunar semi-diurnal components, J. Geophys. Res. 87:5241-5252.

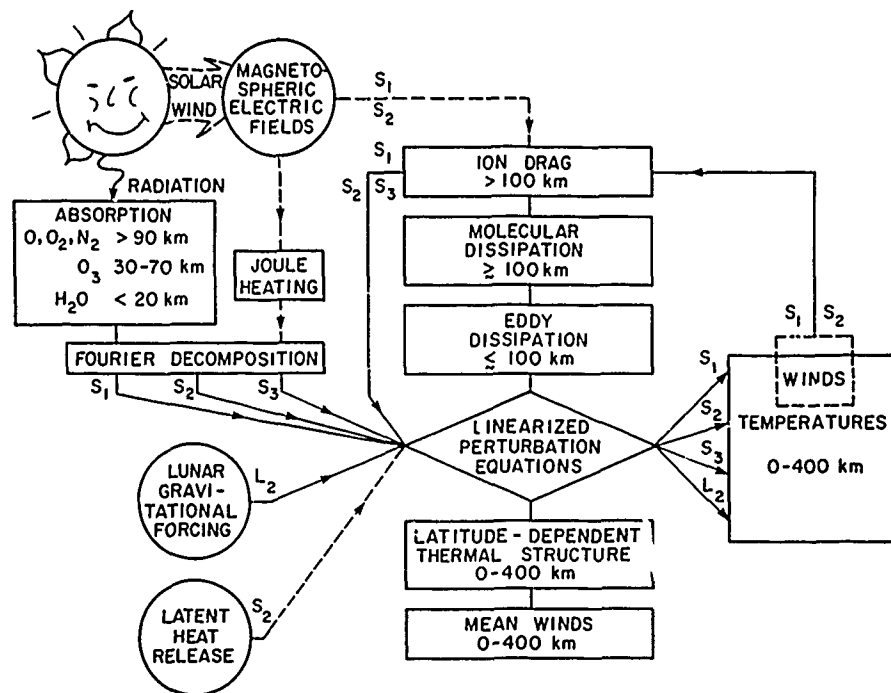


Figure 1. Schematic Describing the Numerical Model of Atmospheric Tides Developed by Forbes<sup>1,2</sup>

Diurnal heating profiles for UV and EUV absorption used in the Forbes<sup>1</sup> model are illustrated in Figure 2. Due to uncertainties in the EUV solar flux, the model is calibrated to yield a diurnal exospheric temperature amplitude of 110 K for a mean exospheric temperature of 1000 K for equinox conditions at Millstone Hill (Oliver<sup>3</sup>). The upper and lower peaks illustrated in Figure 2 are due to EUV and UV absorption, respectively. In addition, the increase in altitude of the peaks as the zenith angle ( $\chi$ ) increases is clearly evident. For an overhead sun ( $\chi = 0$ ) the UV and EUV absorption peaks lie at  $Z \approx 100$  km and  $Z \approx 130$  km, respectively, with corresponding peak total heating rates of  $5.0 \times 10^{-7} \text{ J m}^{-3} \text{ sec}^{-1}$  and  $1.66 \times 10^{-8} \text{ J m}^{-3} \text{ sec}^{-1}$ . The total height-integrated heat inputs for  $\chi = 0$  correspond to values of  $\overline{\epsilon F_{\infty}} \approx 8.3 \text{ ergs cm}^{-2} \text{ sec}^{-1}$  and  $\overline{\epsilon F_{\infty}} \approx 0.70 \text{ ergs cm}^{-2} \text{ sec}^{-1}$ , for UV and EUV excitations, respectively, where  $\epsilon$  is the heating efficiency,  $F_{\infty}$  is the unattenuated solar flux, and the overbar represents an average over the relevant wavelength bands. While it is recognized

3. Oliver, W. L. (1980) Improved Millstone Hill exospheric temperature measurements: evidence for a seasonal variation of the magnetic activity effect, *J. Geophys. Res.* 85:4237-4247.

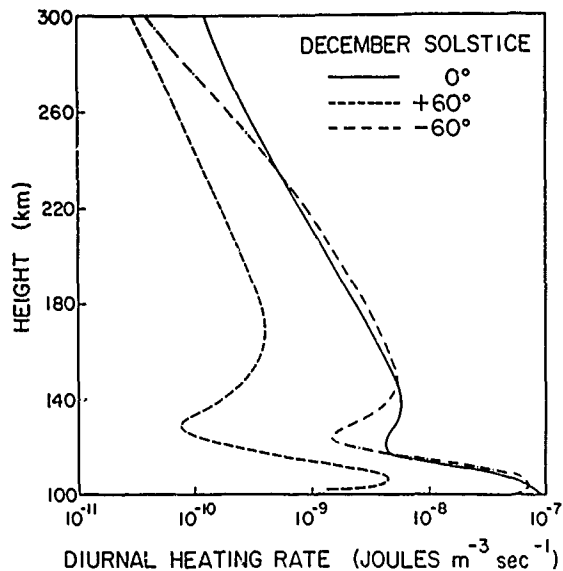


Figure 2. Diurnal Heating Rates Due to UV and EUV Absorption in the Thermosphere (Forbes<sup>1,2</sup>)

the  $\epsilon$  may exhibit some height dependence (Torr et al<sup>4</sup>), this does not appreciably affect values of the integrated heat input quoted previously.

Figure 3 illustrates amplitude and phase vertical structures at  $-18^\circ$ ,  $18^\circ$ ,  $-42^\circ$ , and  $42^\circ$  latitude for the solar diurnal westerly wind at December solstice from the Forbes<sup>1</sup> model. The following features are worth noting:

(1) Below 100 km at low latitudes the exponential amplitude growth and phase progression ( $\lambda_z \approx 30$  km) with height are characteristic of the (1, 1) diurnal propagating tide. The (1, 1) mode attains its peak amplitudes near 110 km and decays rapidly above this height due to molecular dissipation.

(2) Below 100 km at high latitudes the relative absence of amplitude growth and phase progression with height is indicative of the (1, -2) trapped mode. Superposition of the (1, 1) and (1, -2) modes accounts for the illustrated changes in vertical structure of the diurnal tidal winds and temperatures.

(3) Amplitudes and phases of  $u$ ,  $v$ , and  $\delta T$  are asymptotic to constant values above 200 km. This behavior is consistent with the dominance of diffusion in the upper thermosphere, and with the condition that there be no sources of heat or momentum in the upper thermosphere.

4. Torr, M.R., Richards, R.G., and Torr, D.G. (1980) A new determination of the ultra-violet heating efficiency of the thermosphere, J. Geophys. Res. 85:6819-6326.

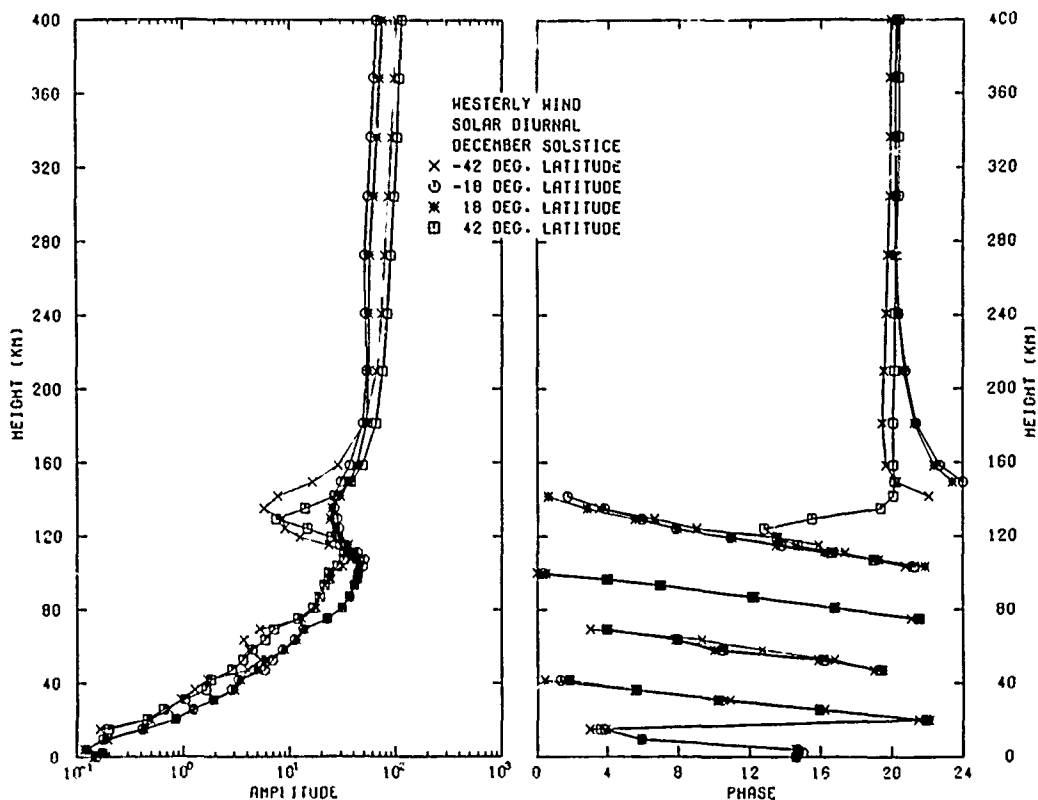


Figure 3. Solar Diurnal Solstitial Westerly Winds From the Forbes<sup>1</sup> Model Corresponding to  $T_0 = 1000$  K

(4) Diurnal tidal oscillations in the 90-150 km region receive about equal contributions from upward propagating and in situ excited components.

Item (4) is examined in detail in Figure 4 where the northerly velocity at 18° latitude is separated into relative contributions due to the (1, 1) propagating tide (predominant below 150 km) and that excited in situ by UV and EUV solar radiation absorption (predominant above 150 km). These results permit interpretation of tidal measurements of the northerly wind at Arecibo (18°N) (Harper<sup>5</sup>) as illustrated in Figure 5, which are in excellent agreement with the Forbes<sup>1</sup> model. Note the transition from a 30-km vertical wavelength phase progression with height below 150 km [indicative of the (1, 1) model] to phase and amplitude constancy with height indicative of fast molecular diffusion and in situ excitation.

5. Harper, R.M. (1981) Some results on mean tidal structure and day-to-day variability over Arecibo, *J. Atmos. Terr. Phys.* 43:255-262.

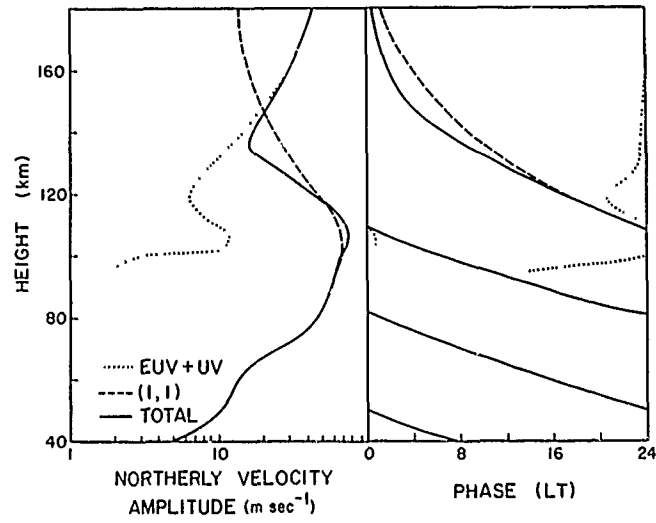


Figure 4. Northerly Velocity at 18° Latitude Due to In Situ Excitation, the Propagating (1, 1) Mode, and the Sum of These Sources

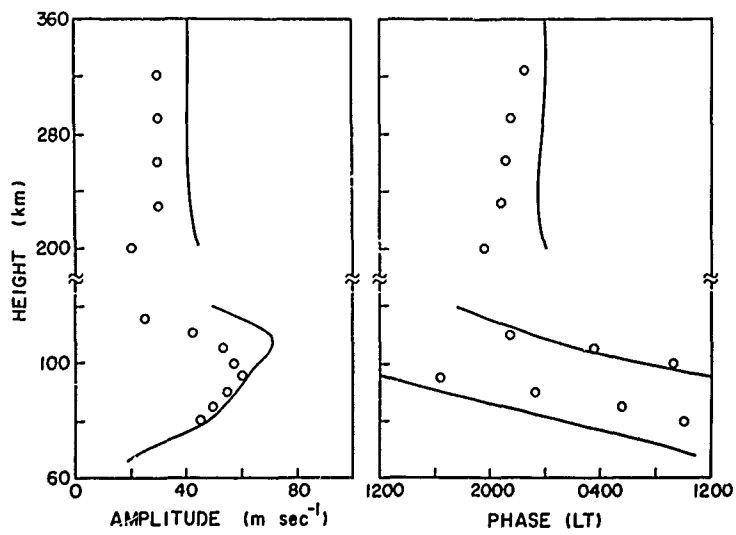


Figure 5. Diurnal Northerly Velocities at Arecibo (18°N) (Harper<sup>5</sup>) Compared With the Forbes<sup>1</sup> Model

As discussed in the preceding paragraph, thermospheric models are often tuned to yield observed diurnal temperature amplitudes. This is possible since the diurnal thermospheric tide is excited almost exclusively in situ and is sufficiently large that a reliable experimental determination of its amplitude can be made. The shape of the local time variation of heating at a given height and latitude, which depends on the thermal and compositional structure of the background atmosphere, in turn fixes the amplitude of the semidiurnal component relative to the diurnal component. Semidiurnal heating rates in the thermosphere constructed in this manner (Forbes<sup>2</sup>) are illustrated in Figure 6. Note that heating rates at all levels are not necessarily in phase, depending upon whether the region is optically thin (higher altitudes) or optically thick (lower altitudes). Figures 1 and 6 may be compared to the heating profiles utilized by Dickinson et al<sup>6</sup> in their thermospheric general circulation model, which exhibit the same characteristics as described above, as illustrated in Figure 7.

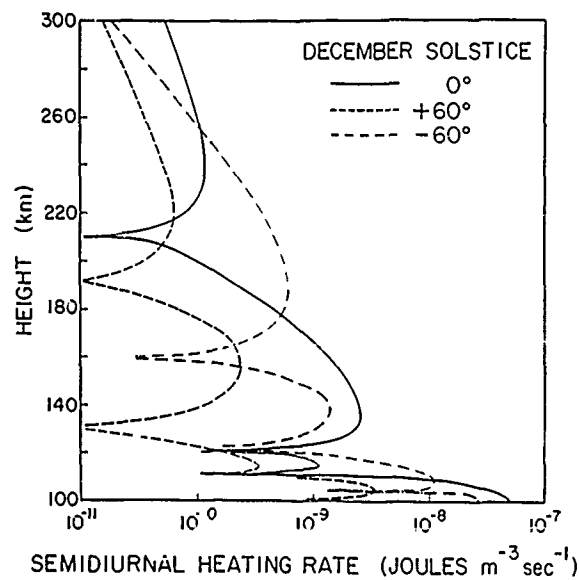


Figure 6. Semidiurnal Heating Rates Due to UV and EUV Absorption in the Thermosphere (Forbes<sup>1,2</sup>)

6. Dickinson, R. E., Ridley, E. C., and Roble, R. G. (1981) A three-dimensional general circulation model of the thermosphere, J. Geophys. Res. 86:1499-1512.

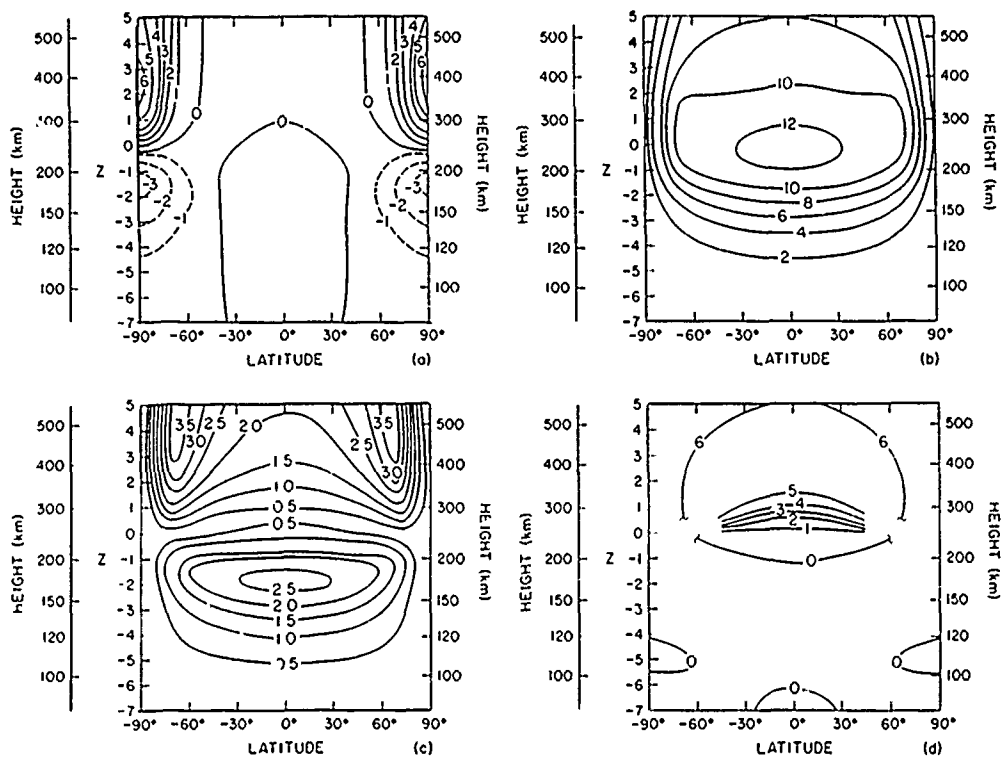


Figure 7. Global Fourier Decomposition of the Perturbation Solar Heating Distribution for Equinox Conditions During Solar Cycle Maximum (a) Zonal mean values for perturbation heating, (b) amplitude of wave number 1 (phase of 1200 LT), (c) amplitude of wave number 2, and (d) phase of wavenumber 2. The units of amplitude are  $\text{J kg}^{-1} \text{sec}^{-1}$ , and the phase is the time of the maximum in hours (Dickinson et al<sup>6</sup>)

Correlation between diurnal winds and diurnal ion drag when treated in a linear system enters as a semidiurnal momentum source in the thermosphere, as illustrated in Figure 8. In addition, semidiurnal propagating tides excited by  $\text{H}_2\text{O}$  and  $\text{O}_3$  insolation absorption can effectively penetrate into the thermosphere and contribute to the total semidiurnal variation. Figure 9 illustrates a Hough mode decomposition of the numerical calculations of Forbes<sup>2</sup> for the semidiurnal tides excited below 100 km. Semidiurnal tides are excited indirectly by "mode coupling" due to interaction of the main (2, 2) mode with background winds. Note that between 60 and 90 km (2, 2) exhibits an evanescent nature, whereas the higher-order (2, 3), (2, 4), and (2, 5) modes grow exponentially with height; all four modes are comparable in the meteor wind region (80-100 km). The (2, 4) mode becomes dominant in the E-region (100-140 km), but is secondary to the (2, 2) mode above 150 km. This behavior is indicative of the preferential damping of the shorter-wavelength (2, 4) and (2, 5) modes.

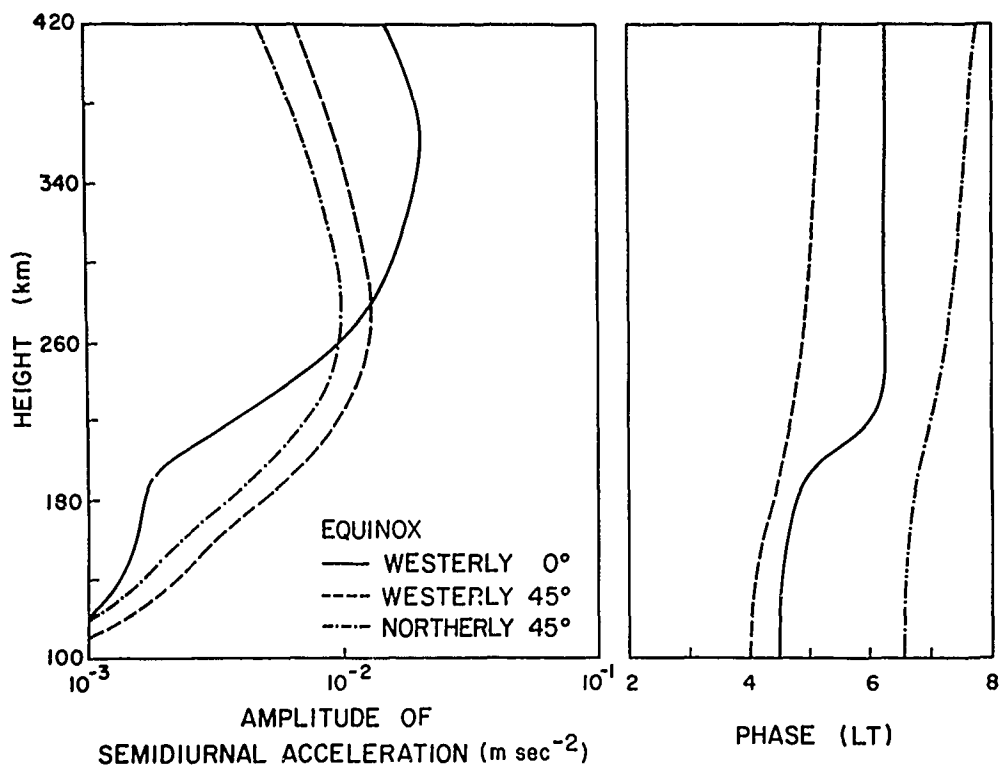


Figure 8. Semidiurnal Acceleration Due to Coupling Between Diurnal Winds and Diurnal Ion Drag (Forbes<sup>2</sup>)

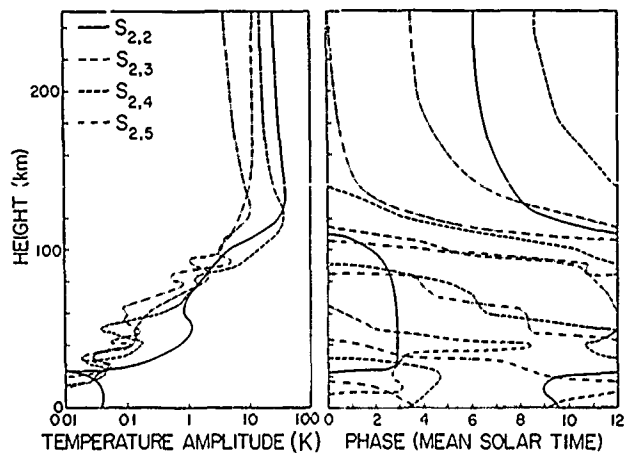


Figure 9. Hough Mode Decomposition of Semidiurnal Temperatures at Solstice Due to Tides Excited by  $\text{H}_2\text{O}$  and  $\text{O}_3$  Insolation Absorption (Forbes<sup>2</sup>)

The nonlinear coupling between tidal winds and ion drag has been invoked by Mayr et al<sup>7</sup> to explain spurious anomalous increases observed in the equatorial neutral temperature around midnight by the NATE\* experiment on AE-E, as illustrated in Figure 10. Figure 11 illustrates the semidiurnal and terdiurnal tidal variations in N<sub>2</sub> and temperature due to various excitation mechanisms. The semidiurnal component receives strong contributions from (a) diurnal winds interacting with the diurnal ion drag (see Figure 8), and (b) upward propagating modes excited by O<sub>3</sub> insolation absorption (see Figure 9). The semidiurnal fields interacting with the diurnal component of ion drag, in turn, generate a substantial terdiurnal component. The synthesis of all contributions yields the signature of a midnight temperature maximum in the upper thermosphere as illustrated in Figure 12.

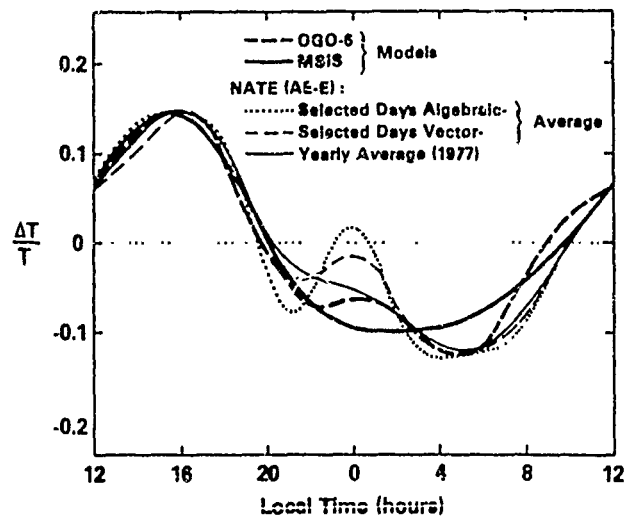


Figure 10. Comparisons Between OGO-6 and MSIS Models at 250 km and Fourier Analyzed In Situ T<sub>g</sub> Measurements From the NATE Experiment on AE-E (Mayr et al<sup>7</sup>)

\* Neutral Atmosphere Temperature Experiment

7. Mayr, H.G., Harris, I., Spencer, N.W., Hedin, A.E., Wharton, L.E., Porter, H.S., Walker, J.C.G., and Carlson, H.C. (1979) Atmospheric tides and the midnight temperature anomaly, Geophys. Res. Lett. 6:447-450.

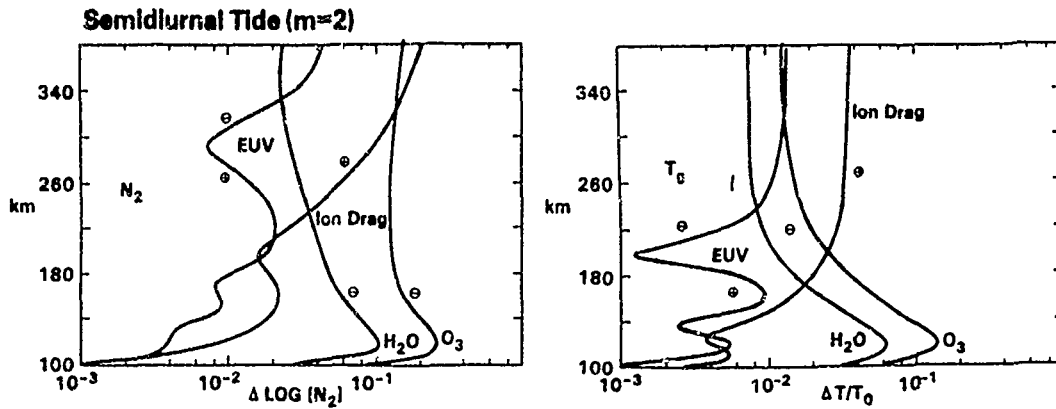


Figure 11a. Semidiurnal Tides for  $T_g$  and  $N_2$  Density Associated With Various Excitation Mechanisms. Plus and minus signs indicate phase in quadrants near 00(12) and 06(18) local times, respectively

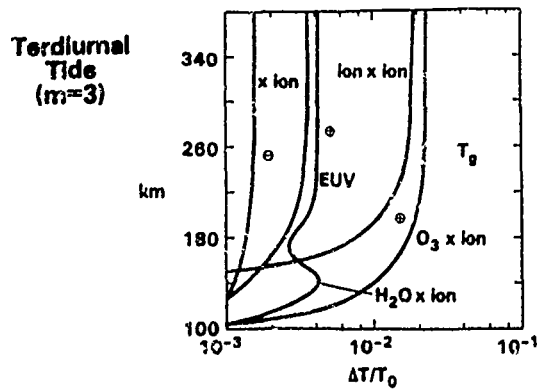


Figure 11b. The Terdiurnal Component for the Temperature. Plus and minus signs indicate phase in quadrants near 00(08) and 04(12) local times, respectively. Except for the EUV contribution the terdiurnal components are the result of nonlinear interactions between semidiurnal wind fields (due to EUV, ion drag, O<sub>3</sub>, and H<sub>2</sub>O) and diurnal variations in the ion density (Mayr et al<sup>7</sup>)

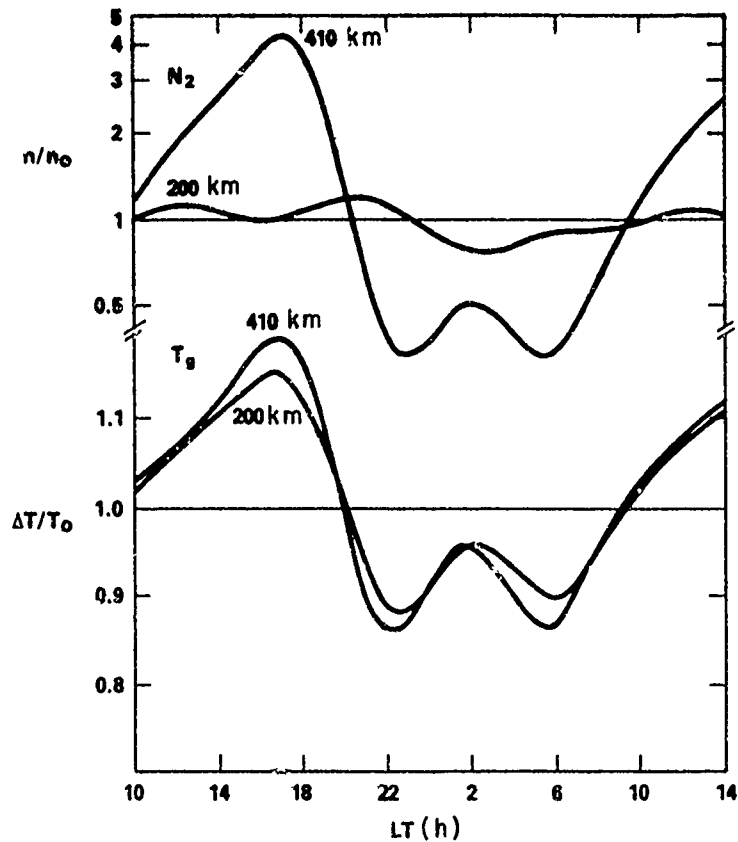


Figure 12. Theoretical Diurnal Variations of Temperature and  $N_2$  Density. Note that at 200 km  $N_2$  does not yet show the signature of a nighttime temperature maximum (Mayr et al<sup>7</sup>)

The joint presence of molecular viscosity, thermal conductivity, anisotropic ion drag, and rotation on a sphere renders the viscid tidal equations inseparable with respect to height and latitude, whereas in an inviscid atmosphere where the background temperature is independent of latitude the equations are separable, and classical tidal theory applies. In classical tidal theory the eigensolutions (Hough functions) of Laplace's tidal equation define the horizontal structures of each mode, and the eigenvalues (equivalent depths) fix each mode's vertical structure. Thus, besides alteration of the vertical tidal structures from exponential growth (for propagating tides) or decay (for trapped tides) to asymptotically constant solutions in the upper thermosphere, the region where  $\chi$ , the ratio of the wave period to the dissipative time scale, approaches unity is also characterized by a transition from tidal solutions that are separable with respect to height and latitude to one in which vertical structures for a particular "modal extension" into

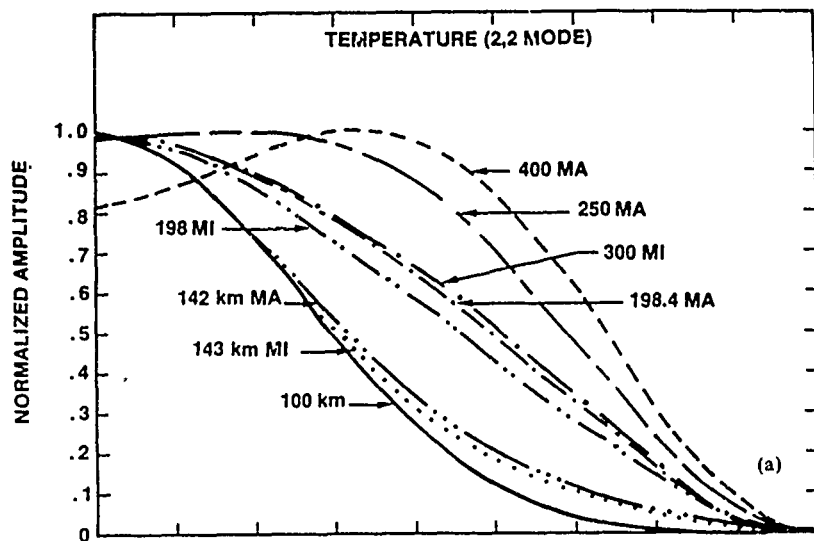


Figure 13a. Amplitude of Temperature Oscillation of the (2, 2) Hough Mode Extension as a Function of Latitude for Selected Altitudes and Sunspot Conditions (Values Normalized by Maximum Value at Each Altitude). MI refers to sunspot minimum; MA refers to sunspot maximum. Values at 100 km are assumed to be independent of sunspot conditions (Lindzen et al<sup>8</sup>)

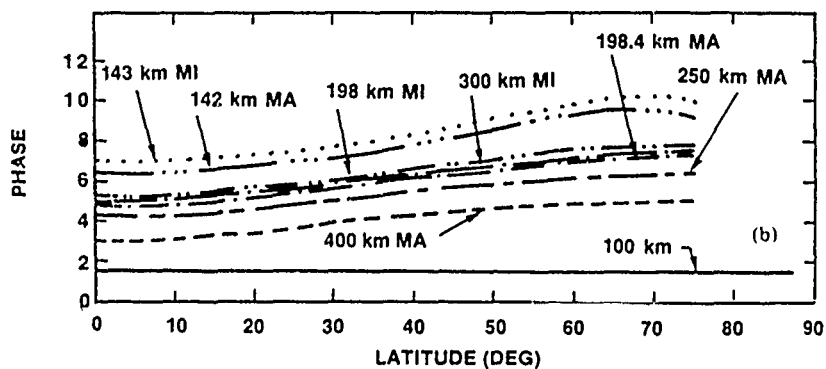


Figure 13b. Phase of Temperature Oscillation (Time of Maximum, Local Time) of the (2, 2) Hough Mode Extension as a Function of Latitude for Selected Altitudes and Sunspot Conditions (Lindzen et al<sup>8</sup>)

8. Lindzen, R.S., Hong, S., and Forbes, J.M. (1977) Semidiurnal Hough mode extensions into the thermosphere and their application, NRL Memorandum Rept. 3442, Naval Research Laboratory, Washington, D.C.

the thermosphere vary with latitude or, equivalently, in which horizontal structures vary with height. This behavior is illustrated in Figures 13 and 14, which depict the horizontal shapes of the (2, 2) and (2, 4) Hough mode extensions (HME) of the semidiurnal temperature oscillation at various heights and levels of solar activity. Note that the node at  $15^\circ$  latitude for (2, 4) disappears and the (2, 2) horizontal shape broadens considerably at progressively greater heights in the thermosphere.

Amplitude and phase vertical structures at  $-18^\circ$ ,  $18^\circ$ ,  $-42^\circ$ , and  $42^\circ$  latitude for the solar semidiurnal westerly wind at December solstice from the Forbes<sup>2</sup> model are illustrated in Figure 15. The transition to shorter vertical wavelengths between 80 and 100 km, the effects of dissipation on the upward propagating components between 110 and 150 km, and the asymptotic behavior characteristic of the upper thermosphere are clearly illustrated. The upper thermosphere velocity and temperature fields, which typically range between  $10\text{-}50\text{ m sec}^{-1}$  and  $20\text{-}40\text{ K}$  with the larger values at low latitudes, originate with about equal weighting from three excitation sources: (1) in situ EUV excitation, (2) ion-drag momentum coupling with the diurnal tidal winds, and (3) upward propagating modes excited below 100 km. Figure 16 illustrates the consistency of the model calculations with measurements of the northerly wind between 120 and 180 km at Arecibo (Harper<sup>5</sup>).

Global Fourier decomposition of the perturbation meridional wind from the thermospheric circulation model of Dickinson et al,<sup>6</sup> as shown in Figure 17, can be compared with the Arecibo data and Forbes<sup>1,2</sup> model results in Figures 5 and 16. The diurnal winds above 200 km as computed by Dickinson et al<sup>6</sup> underestimate the observed ( $30\text{ m sec}^{-1}$ ) values by about  $10\text{ m sec}^{-1}$  and predict a phase that is  $\sim 2\text{-}3\text{ h}$  later than the observed 2200 h. The absence of an upward-propagating (1, 1) mode in their model is clearly evident below 150 km. The semidiurnal winds similarly indicate values ( $\sim 10\text{ m sec}^{-1}$ ) that, when compared to observations ( $\sim 40\text{-}60\text{ m sec}^{-1}$ ), clearly indicate the importance of upward-propagating tidal components that they have neglected. The NCAR\* general circulation model is, however, in the process of being modified to alleviate this shortcoming (Roble<sup>9</sup>).

The lunar semidiurnal counterparts of Figures 15 and 9 are given in Figures 18 and 19, respectively. Although the lunar gravitational excitation consists of some (2, 4) in addition to the predominant (2, 2) forcing, the excitation of the higher-order (2, 4) and (2, 5) modes are due almost exclusively to mode coupling due to mesospheric mean winds and meridional temperature gradients. Winds

---

\*National Center for Atmospheric Research.

9. Roble, R.G. (1982) Private communication.

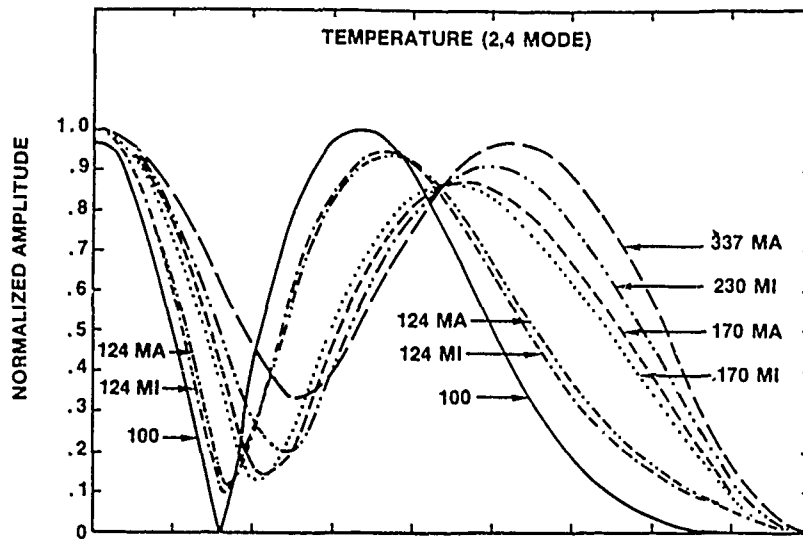


Figure 14a. Amplitude of Temperature Oscillation of the (2, 4) Hough Model Extension as a Function of Latitude for Selected Altitudes and Sunspot Conditions (Values Normalized by Maximum Value at Each Altitude). MI refers to sunspot minimum; MA refers to sunspot maximum. Values at 100 km are assumed to be independent of sunspot conditions (Lindzen et al<sup>8</sup>)

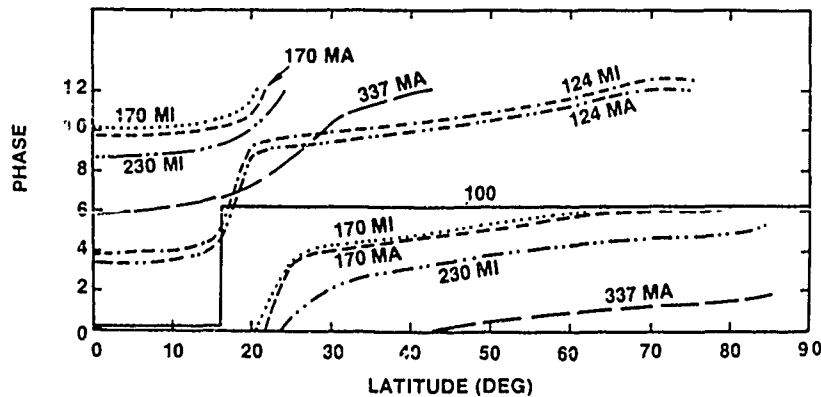


Figure 14b. Phase of Temperature Oscillation (Time of Maximum, Local Time) of the (2, 4) Hough Mode Extension as a Function of Latitude for Selected Altitudes and Sunspot Conditions (Lindzen et al<sup>8</sup>)

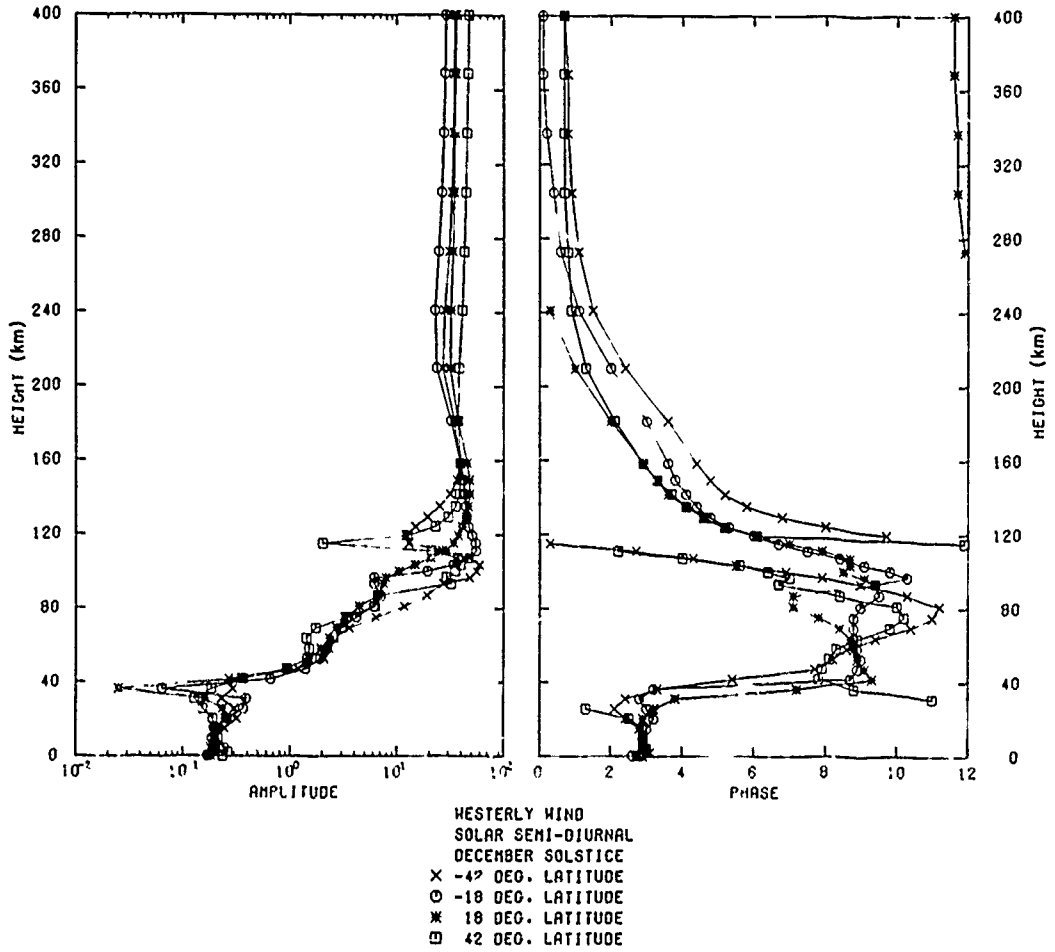


Figure 15. Solar Semidiurnal Solstitial Westerly Winds From the Forbes<sup>1</sup> Model Corresponding to  $T_0 = 1000$  K

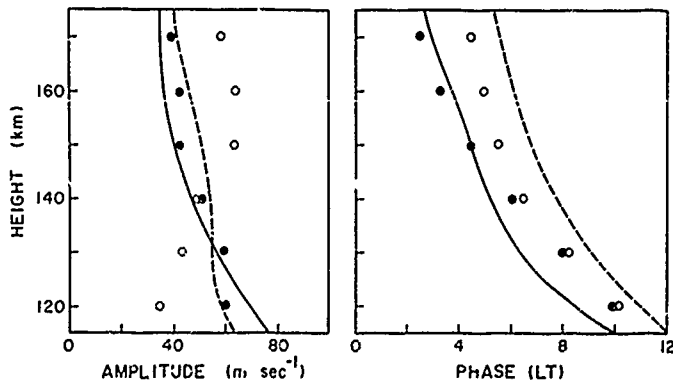


Figure 16. Solar Semidiurnal Northerly Velocities at Arecibo ( $18^{\circ}$ N) (Harper<sup>5</sup>) Compared With the Forbes<sup>1</sup> Model

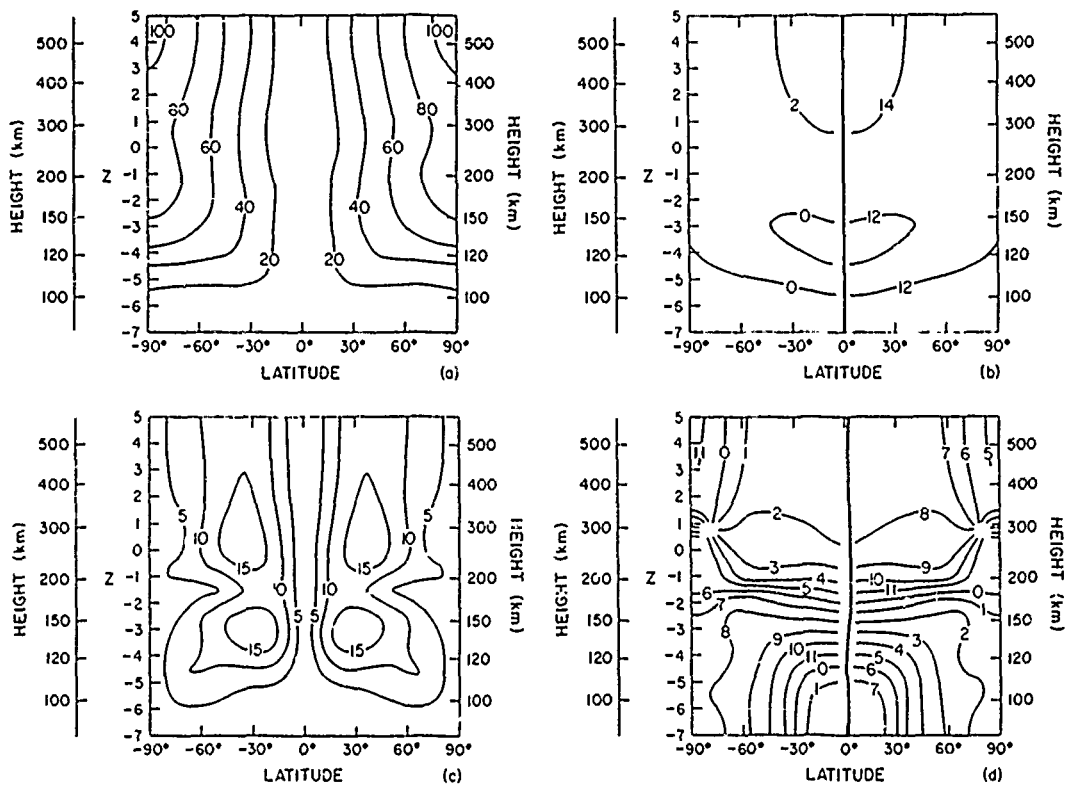


Figure 17. Global Fourier Decomposition of Perturbation Meridional Wind ( $\text{m sec}^{-1}$ ) for Equinox Conditions During Solar Cycle Maximum. Both solar and high-latitude heating are included in the model calculation: (a) amplitude of wave number 1, (b) phase of wave number 1, (c) amplitude of wave number 2, and (d) phase of wave number 2 (Dickinson et al<sup>6</sup>)

(temperatures), in fact, reach amplitudes of order  $10\text{-}15 \text{ m sec}^{-1}$  ( $10\text{-}15 \text{ K}$ ) in lower thermosphere, and  $5\text{-}10 \text{ m sec}^{-1}$  ( $5\text{-}10 \text{ K}$ ) in the upper thermosphere, and may thus account for a significant portion of day-to-day variability reported in measurements of the solar semidiurnal tide. This calculation confirms the excitation of higher-order lunar modes as anticipated by Evans.<sup>10</sup>

10. Evans, J. V. (1978) A note on lunar tides in the ionosphere, J. Geophys. Res. 83:1647-1652.

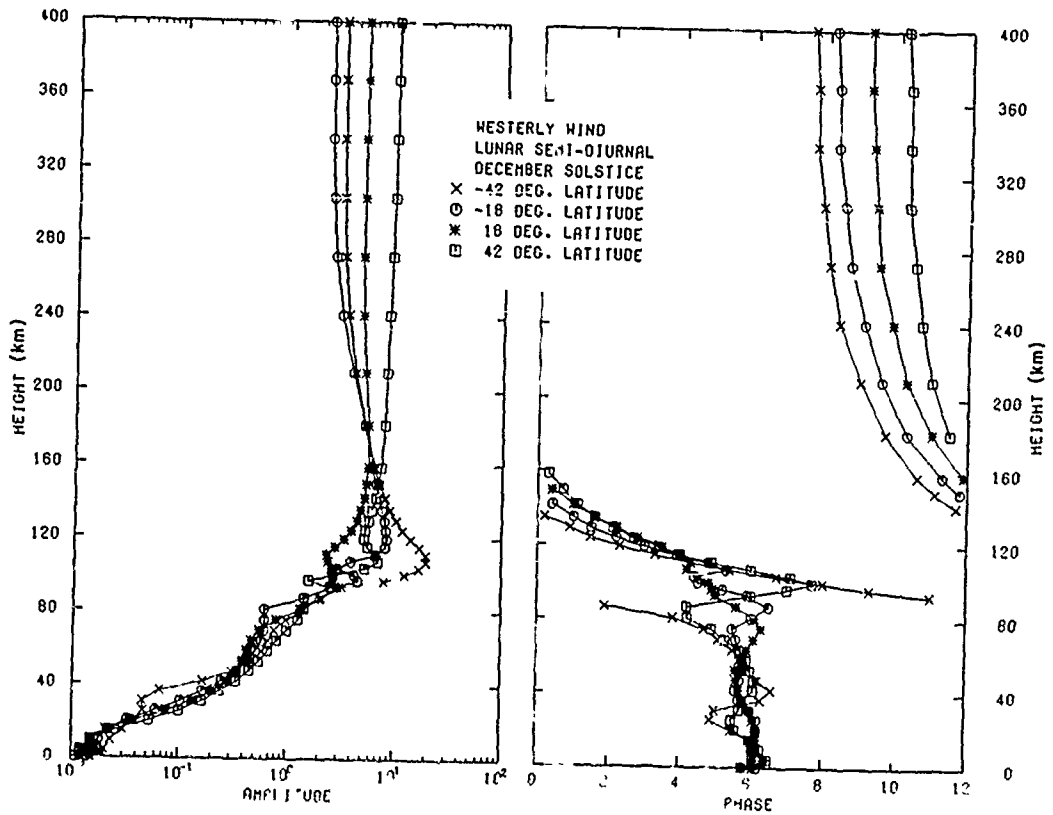


Figure 18. Lunar Semidiurnal Solstitial Westerly Winds From the Forbes<sup>1</sup> Model Corresponding to  $T_0 = 1000$  K

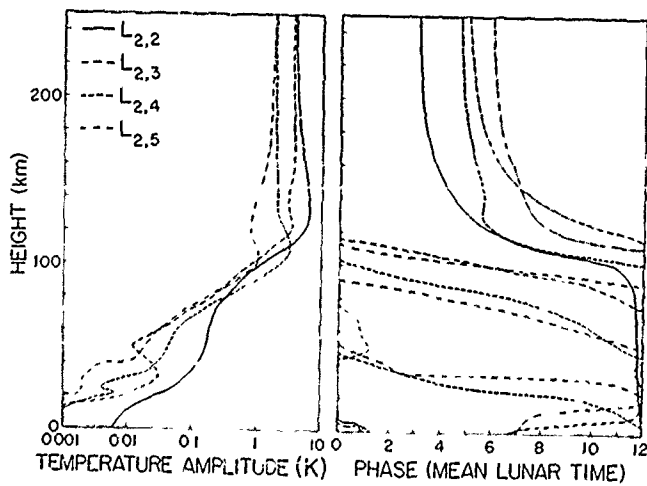


Figure 19. Hough Mode Decomposition of Semidiurnal Temperatures at Solstice Due to Lunar Semidiurnal Tide Excited by Gravitational Forcing

## 2. TIDES FROM THOMSON SCATTER MEASUREMENTS

An analysis of seasonal and solar cycle variations in neutral exospheric temperatures ( $T_{\infty}$ ) from Thomson scatter measurements at Millstone Hill has recently been performed by Hagan et al.<sup>11</sup> Figures 20 and 21 illustrate the diurnal behavior of  $T_{\infty}$  at Millstone Hill for a typical solar maximum day ( $F_{10.7} = 257$ ; Figure 20) and a typical solar minimum day ( $F_{10.7} = 81$ ; Figure 21), both during quiet geomagnetic conditions. A stepwise least squares technique is used to fit the data such that only the statistically significant harmonic components are retained. Note that Figure 20 is adequately fitted by only a 24-h period wave, whereas in Figure 21 that 12-h and 8-h periods are clearly present in the data.

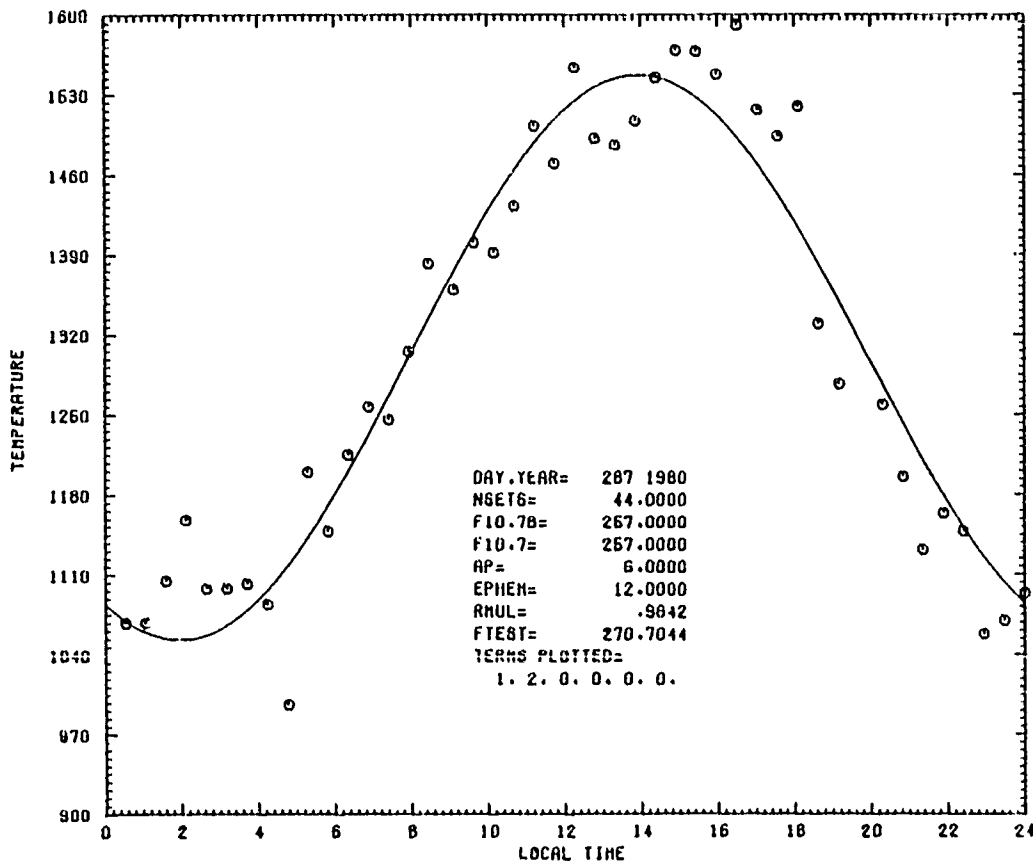


Figure 20. Example of Millstone Hill Neutral Exospheric Temperature Data During a Magnetically Quiet Day at Solar Maximum

11. Hagan, M. E., Forbes, J. M., Satyanarayana, P., and Oliver, W. (1982) Exospheric temperatures at Millstone Hill: An interim analysis (in preparation).

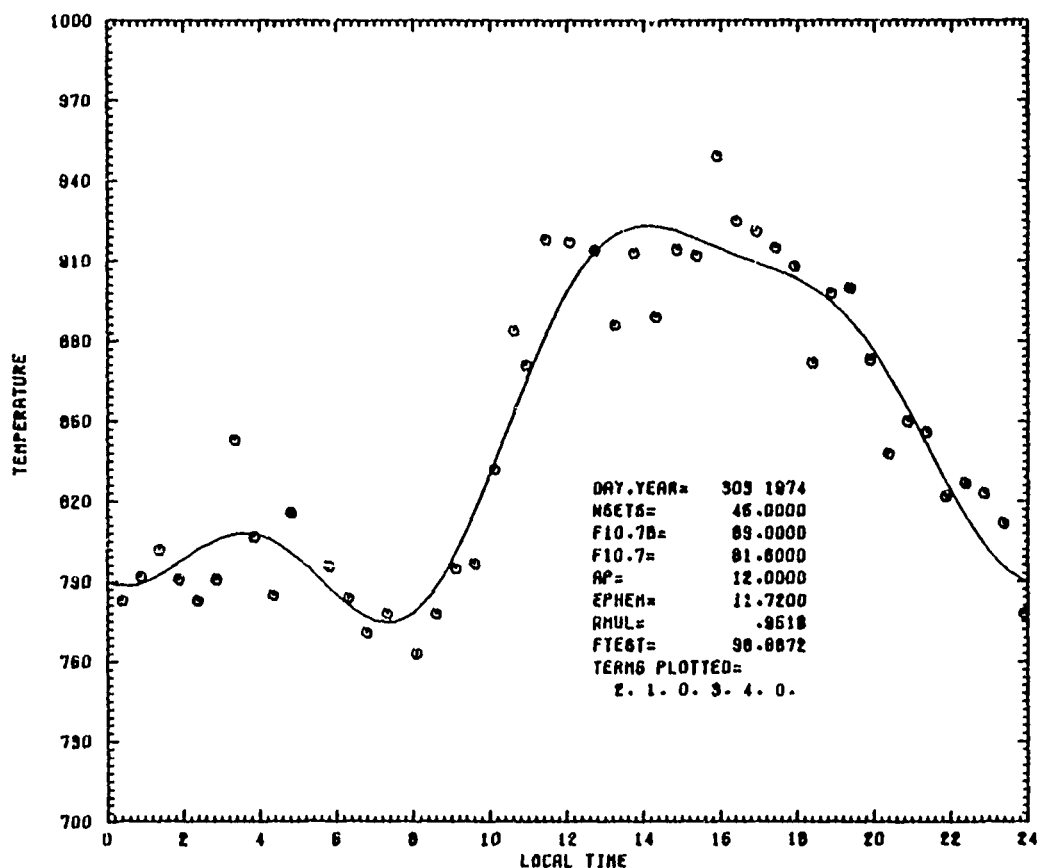


Figure 21. Example of Millstone Hill Neutral Exospheric Temperature Data During a Magnetically Quiet Day at Solar Minimum

The mean ( $T_0$ ) and diurnal ( $\delta T_1$ ) amplitudes from 40 days of data are plotted in Figures 22 and 23 to illustrate the solar cycle dependents of  $T_0$  and  $\delta T_1$ . The seasonal variability of  $T_0$  is consistent with the temperatures from the theoretical zonal mean circulation model of Roble et al.<sup>12</sup> In addition, the MSIS (Hedin et al.<sup>13, 14</sup>) model (and its extrapolation outside the  $F_{10.7}$  range of its data base indicated by a dashed line in Figures 22 and 23) reproduces the solar cycle variation of  $T_0$  quite well. On the other hand, as illustrated in Figure 23, the MSIS model clearly underestimates the measured  $\delta T_1$ 's for levels of solar activity where  $T_0$  is in excess of 1100 K (or equivalently,  $F_{10.7} \geq 175$ ). The phase of the diurnal oscillation of temperature (Figure 24) indicates a

---

References cited above will not be listed here. See References, page 41.

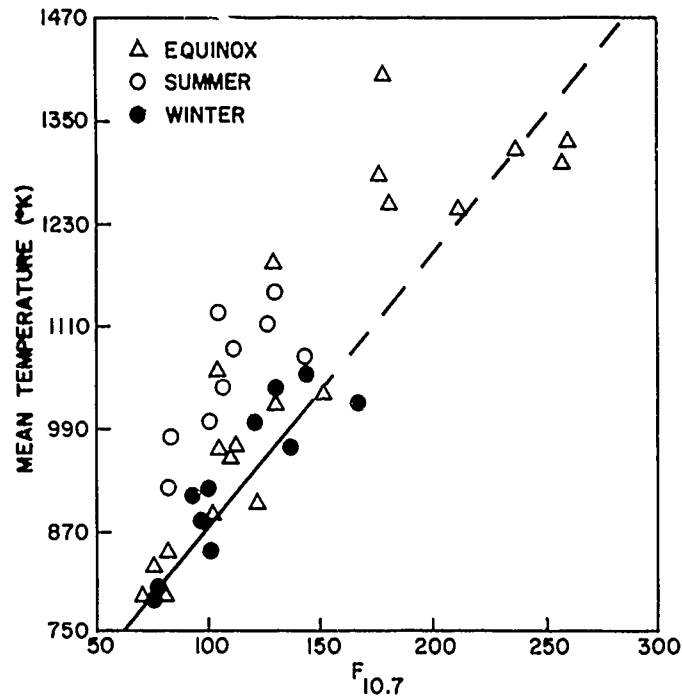


Figure 22. Millstone Hill Diurnal Mean Temperatures vs  $F_{10.7}$  and MSIS Model Prediction. Dashed line represents extension of MSIS model beyond range of  $F_{10.7}$  values for data upon which it was based

transition from  $\sim 15$ - $16$  h during winter months to  $\sim 12$ - $13$  h during summer months. The MSIS model predicts a 2-h phase shift of the correct sense but clearly underestimates the magnitude of the effect.

The semidiurnal temperature amplitudes ( $\delta T_2$ ) inferred from the Millstone Hill Thomson scatter measurements clearly indicate a solar cycle dependence (Figure 25) and a seasonal dependence of the phase (Figure 26), indicating a winter to summer phase shift of +3 h. The MSIS phase shift of 5 h clearly overestimates this effect. The semidiurnal amplitudes of the MSIS model are clearly indicated to be too small.

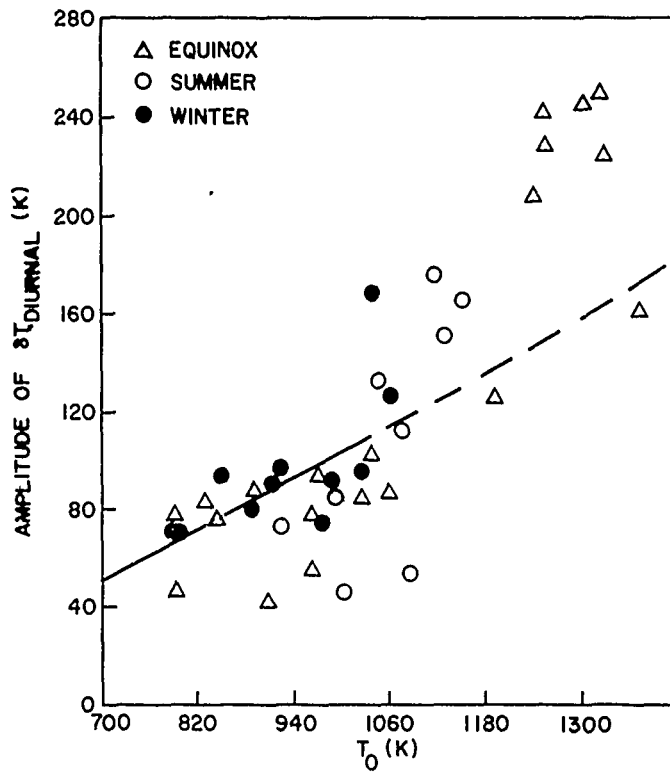


Figure 23. Millstone Hill Diurnal Temperature Amplitudes vs  $T_0$  (Hagan et al<sup>11</sup>). Dashed line represents extension of MSIS model beyond range of  $F_{10.7}$  values for data upon which it was based

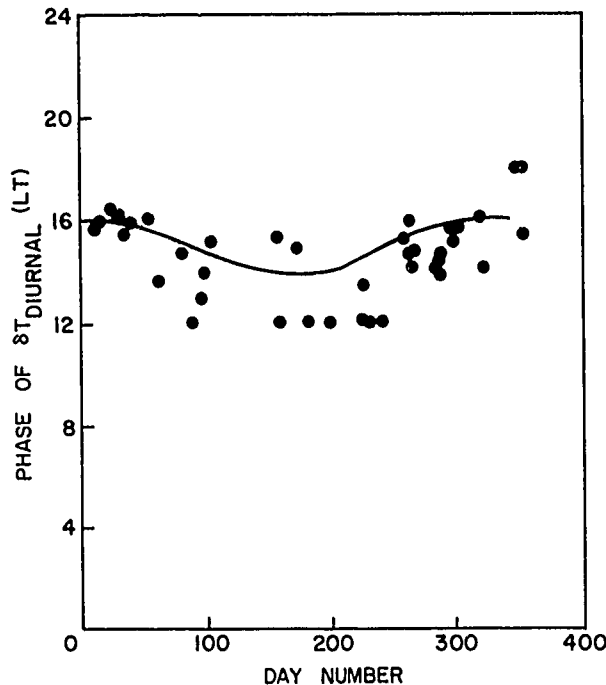


Figure 24. Phase of Diurnal Temperature at Millstone Hill vs Day of Year Compared to MSIS Model (Hagan et al<sup>11</sup>)

### 3. TIDES IN COMPOSITION AND TOTAL MASS DENSITY

Mayr and Harris<sup>15</sup> and Forbes<sup>16</sup> have investigated tidal variations in thermospheric O, O<sub>2</sub>, N<sub>2</sub>, Ar, He, and H using models that take into account the effects of tidal temperatures, horizontal and vertical tidal winds, photo- and ion-chemistry, exospheric transport, and thermal diffusion. Hydrogen tidal variations are dominated by vertical flow due to lateral transport in the exosphere, but wind-induced diffusion is the single most important process for causing deviations from diffusive equilibrium (temperature-dominated) solutions of tidal variations in O, O<sub>2</sub>, N<sub>2</sub>, Ar, and He in the thermosphere. The effects of ion- and photo-chemistry on the variations of O and O<sub>2</sub>, and exospheric transport on He, are found to be of secondary or negligible importance above 120 km. In Figure 27 the diurnal oscillations in O, O<sub>2</sub>, N<sub>2</sub>, Ar, He, and H are plotted vs height at the

15. Mayr, H.G., and Harris, I. (1977) Diurnal variations in the thermosphere -2. Temperature, composition, winds, J. Geophys. Res. 82:2628-2640.
16. Forbes, J.M. (1978) Tidal variations in thermospheric O, O<sub>2</sub>, N<sub>2</sub>, Ar, He, and H, J. Geophys. Res. 83:3691-3698.

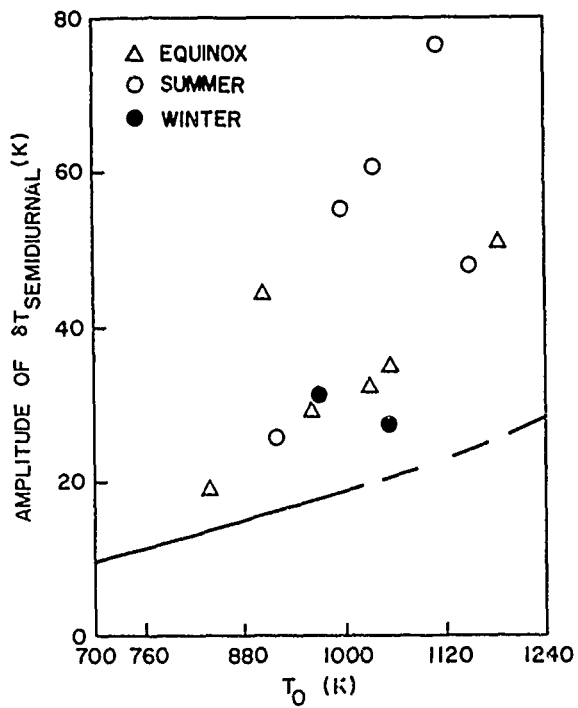


Figure 25. Millstone Hill Semidiurnal Temperature Amplitudes vs  $T_0$  (Hagan et al<sup>11</sup>). Dashed line represents extension of MSIS model beyond range of  $F_{10.7}$  values for data upon which it was based.

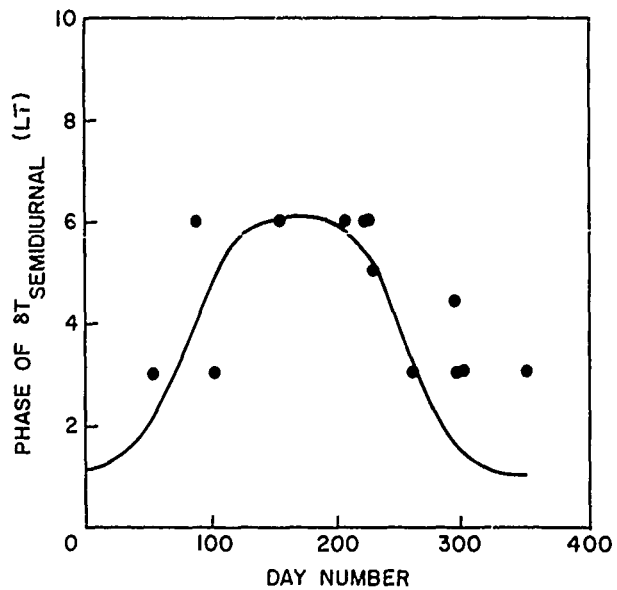


Figure 26. Phase of Semidiurnal Temperature at Millstone Hill vs Day of Year Compared to MSIS Model (Hagan et al<sup>11</sup>)

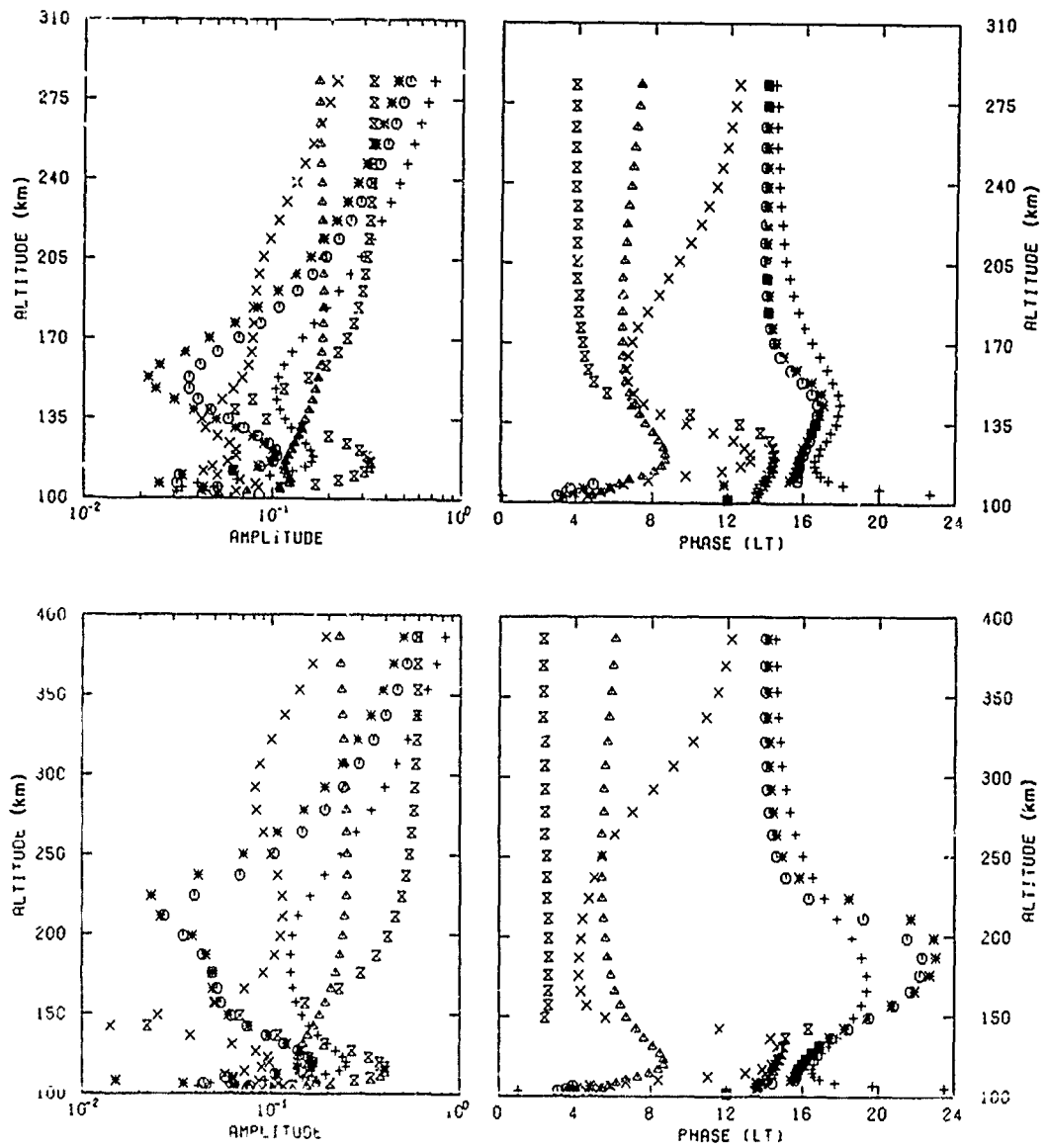


Figure 27. Plots of (Left) Amplitudes and (Right) Phase of Diurnal Variations in O (Crosses), O<sub>2</sub> (Circles), N<sub>2</sub> (Asterisks), Ar (Pluses), He (Triangles), and H (Double Triangles) at (Top) SSMIN and (Bottom) SSMAX at the Equator Under Equinox Conditions (From the Theoretical Model of Forbes<sup>16</sup>)

equator for sunspot minimum (SSMIN) and sunspot maximum (SSMAX) under equinox conditions (Forbes<sup>16</sup>). The phase and amplitude structures for SSMIN agree extremely well with independent calculations by Mayr and Harris.<sup>15</sup> However, the results presented in Figure 27 indicate that solar cycle variations in the diurnal amplitudes and phases of these constituents are likely to be substantial. In particular, the phase difference between O and the heavier constituents (and temperature), which arises mainly due to the effects of winds, extends further into the upper thermosphere during SSMAX than SSMIN. This solar cycle variation of the phase difference simply reflects the fact that diffusion dominates over transport effects at a lower altitude when the mean exospheric temperature is less and should be reflected in the "phase anomaly" of total mass density.

Using the Forbes<sup>16</sup> model with input diurnal winds and temperatures from Forbes and Garrett,<sup>17</sup> Forbes and Marcos<sup>18</sup> calculated the tidal variations in O, N<sub>2</sub>, and total mass density  $\rho$  in the form

$$\ln N = \ln N_0 + \Delta \ln N$$

where  $\ln N_0$  represents a diurnal average value of O, N<sub>2</sub>, or  $\rho$ , and  $\Delta \ln N$  is the tidal perturbation. Determination of total mass density variations from the O and N<sub>2</sub> variations requires a background composition model, and these values were taken from the Jacchia<sup>19</sup> model. In Figure 28 the vertical structures of diurnal amplitude and phase of O, N<sub>2</sub>, and  $\rho$  at equinox are depicted for SSMIN and SSMAX conditions, corresponding to mean exospheric temperatures of 800 K and 1400 K, respectively. Tidal determinations from Atmosphere Explorer E measurements of O and N<sub>2</sub> (Hedin et al.<sup>20</sup>) and total mass density (Forbes and Marcos<sup>21</sup>) are in good agreement with the theoretical predictions of Forbes,<sup>16</sup> which were made independent of the experimental results. The

- 
17. Forbes, J.M., and Garrett, H.B. (1976) Solar diurnal tide in the thermosphere, J. Atmos. Sci. 33:2226-2241.
  18. Forbes, J.M., and Marcos, F.A. (1980) Seasonal-latitude tidal structures of O, N<sub>2</sub> and total mass density in the thermosphere, J. Geophys. Res. 84:3489-3493.
  19. Jacchia, L.G. (1977) Thermospheric Temperature, Density, and Composition: New Models, SAO Special Report 375.
  20. Hedin, A.E., Spencer, N.W., Mayer, H.G., Harris, I., and Porter, H.S. (1978) Direct evidence of transport processes in thermospheric diurnal tide, J. Geophys. Res. 83:3355-3357.
  21. Forbes, J.M., and Marcos, F.A. (1979) Tidal variations in total mass density as derived from the AE-E MESA experiment, J. Geophys. Res. 84:31-35.

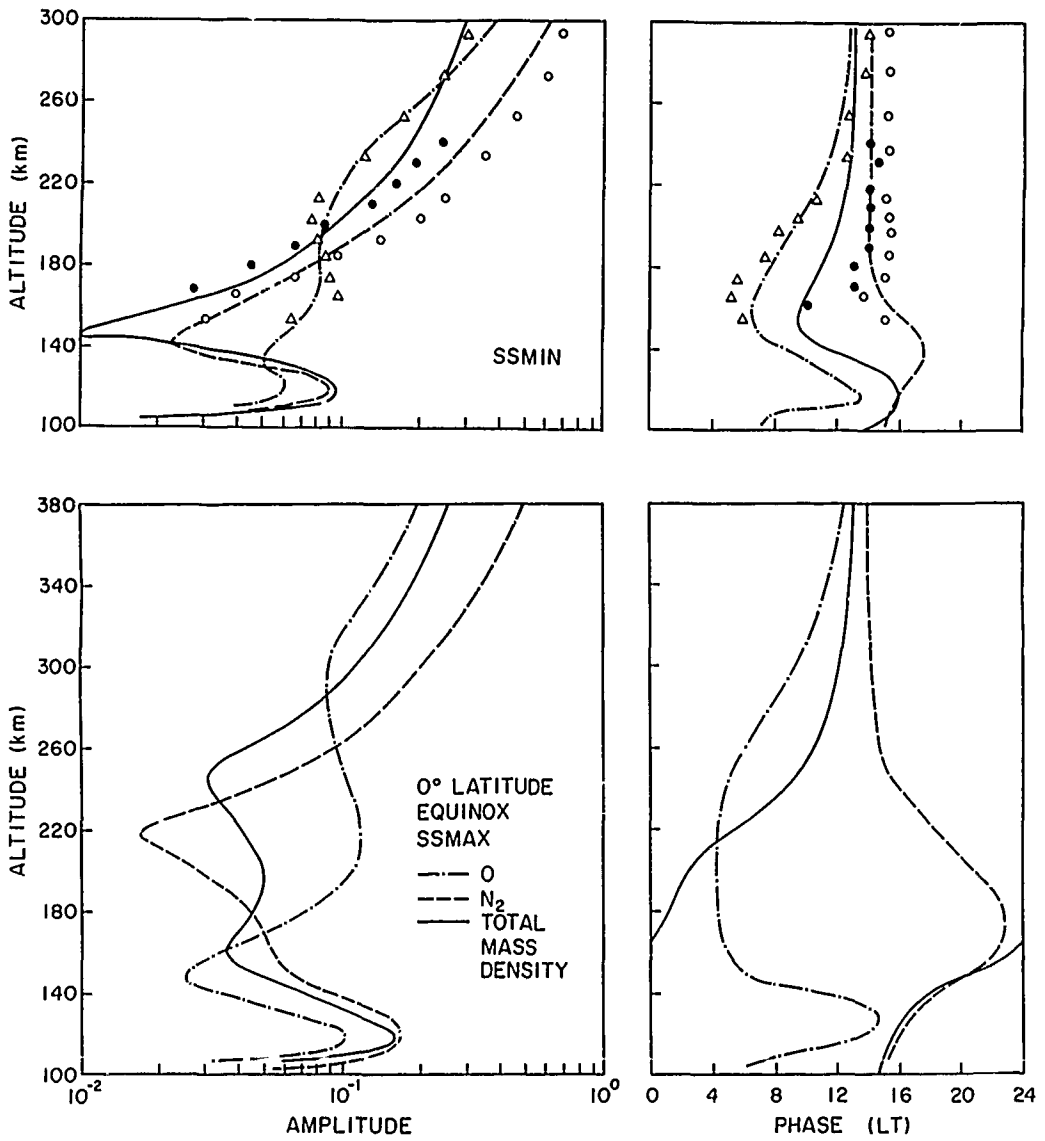


Figure 28. Diurnal Variations in O, N<sub>2</sub>, and Total Mass Density Compared With AE-E Mass Spectrometer o( $\Delta$ ) and N<sub>2</sub>(o), and Accelerometer Total Mass Density ( $\bullet$ ) Measurements (Forbes and Marcos<sup>18</sup>)

only significant discrepancies of the theoretical curves appear to be a 25 percent underestimate of  $N_2$  variations above 200 km and phase predictions that are about 1 h too early above 180 km. Recent calculations that utilize new parameterizations of ion drag, molecular viscosity, thermal conductivity, and background temperature structure (Forbes<sup>1</sup>), do in fact yield a shift in phase of the diurnal temperature amplitude to about 1 h later in local time, in better agreement with the above measurements; amplitudes are generally unaffected, since the solar heat input is calibrated to yield specific diurnal temperature amplitudes at 45°N (80 K at SSMIN and 180 K at SS MAX) consistent with Millstone Hill incoherent scatter measurements.

Basically, the seasonal and latitudinal variations of O in the lower thermosphere (below 200 km) are strongly affected by winds, whereas  $N_2$  at all heights and O about 300 km respond primarily to temperature, which has a different seasonal dependence than the winds. Seasonal and latitudinal variations of  $\rho$  consistent with those of O and  $N_2$  are not obvious, since the extent to which  $\rho$  reflects O and  $N_2$  variations not only depends on the relative amplitudes of O and  $N_2$  but also on their relative molecular weights and background concentrations (O becomes greater than  $N_2$  above 180 km). However, since in general the total mass density must reflect a hydrostatic equilibrium distribution, the profiles of  $\rho$  tend to be similar to the  $N_2$  profiles, with some modification of phase by O, depending on height, season, and solar activity. For instance, since O variations are considerably larger during summer than during winter, the diurnal phase of  $\rho$  during summer consistently lags that during winter by several hours. Further, as pointed out by Forbes and Marcos,<sup>21</sup> the diurnal phase of  $\rho$  between 150 and 200 km is expected on the basis of theory to shift to later times from the equator to mid-latitudes. In an effort to verify this anticipated phase behavior, an extensive data base of total mass densities from accelerometers on four low-altitude satellites (Atmosphere Explorer C, D, and E and Air Force satellite S3-1) was analyzed by Forbes and Marcos.<sup>18</sup> In Figure 29 the "annual average" diurnal phases corresponding to latitude bands 0°-20°, 20°-40°, and 40°-60° derived from the complete data set are compared with theoretical computations at latitudes 10°, 30°, and 50° for equinox conditions at SSMIN. As illustrated, the data and theory do indeed indicate a shift to later times from equatorial to middle latitudes of the diurnal phase of total mass density.

Measurements of neutral composition and temperature aboard the AE-E satellite have also been analyzed to determine the semidiurnal and terdiurnal variations of O,  $N_2$ , He, and Ar from 145-295 km (Hedin et al<sup>22</sup>). The

---

22. Hedin, A. E., Spencer, N. W., and Mayr, H. G. (1980) The semidiurnal and Terdiurnal tides in the equatorial thermosphere from AE-E measurements, J. Geophys. Res. 85:1787-1791.

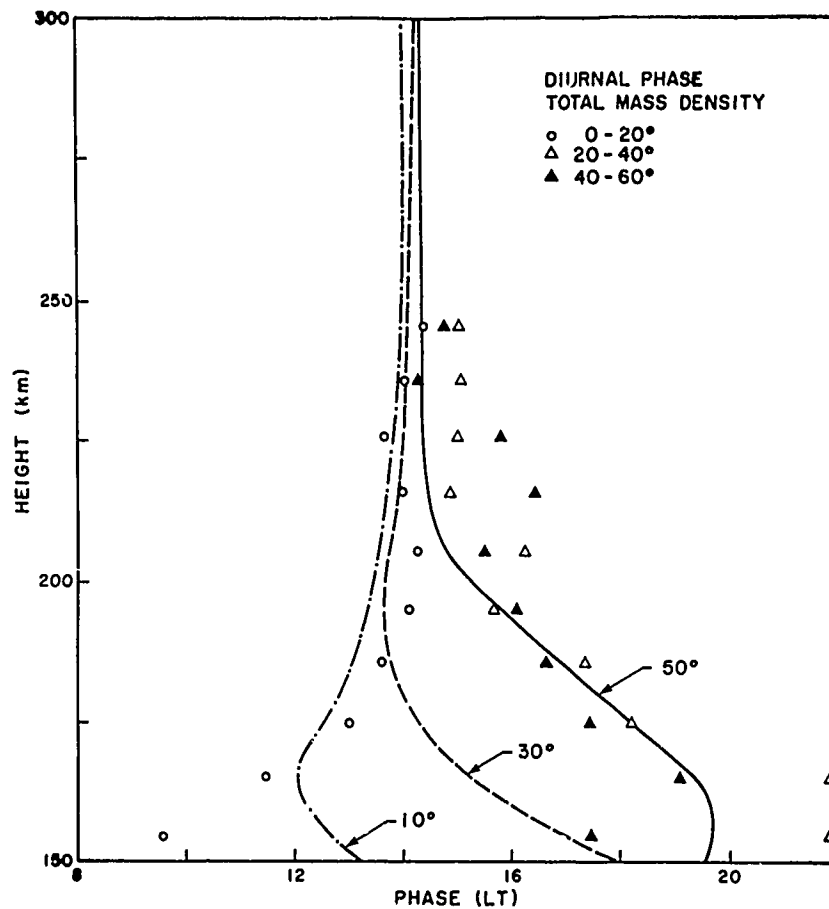


Figure 29. Diurnal Phase of Total Mass Density Compared With Phases Determined From Satellite Accelerometer Measurements (Forbes and Marcos<sup>18</sup>)

semidiurnal variations of O and N<sub>2</sub> are illustrated in Figures 30 and 31, respectively, along with predictions from the MSIS model (Hedin et al<sup>13, 14</sup>), the Forbes<sup>16</sup> model, and the Mayr et al<sup>7</sup> model. For O variations, the Forbes<sup>16</sup> and Mayr et al<sup>7</sup> models predict the overall phase and amplitude structures quite well, with some overestimate of amplitude. Surprisingly, the empirical MSIS does not fit the measurements as well as the theoretical models. On the other hand, the MSIS model provides a much better fit to the semidiurnal amplitude of N<sub>2</sub>, whereas the other models overestimate its amplitude. The semidiurnal phases for N<sub>2</sub> are adequately reproduced by the Forbes<sup>16</sup> and MSIS<sup>13, 14</sup> models, but the Mayr et al<sup>7</sup> model yields phases about 2 h too late above 200 km.

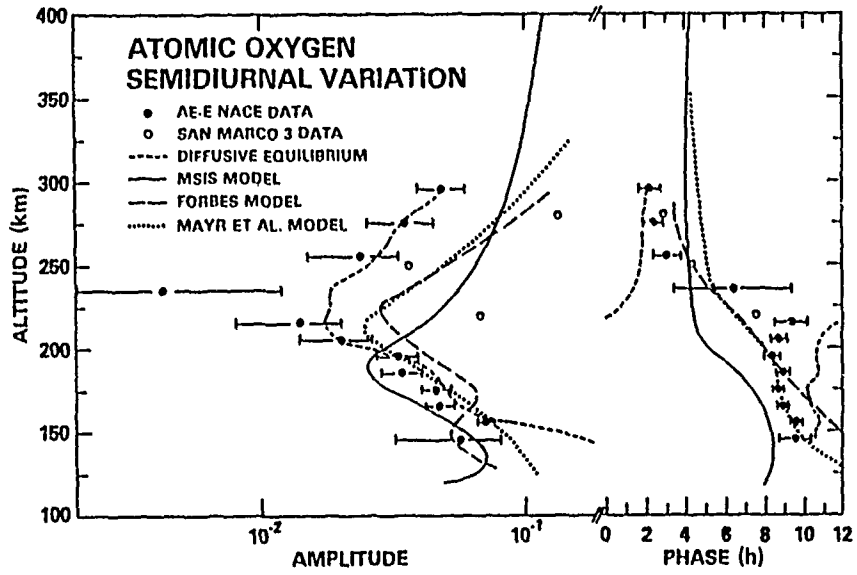


Figure 30. Atomic Oxygen Semidiurnal Variations (Hedin et al<sup>22</sup>)

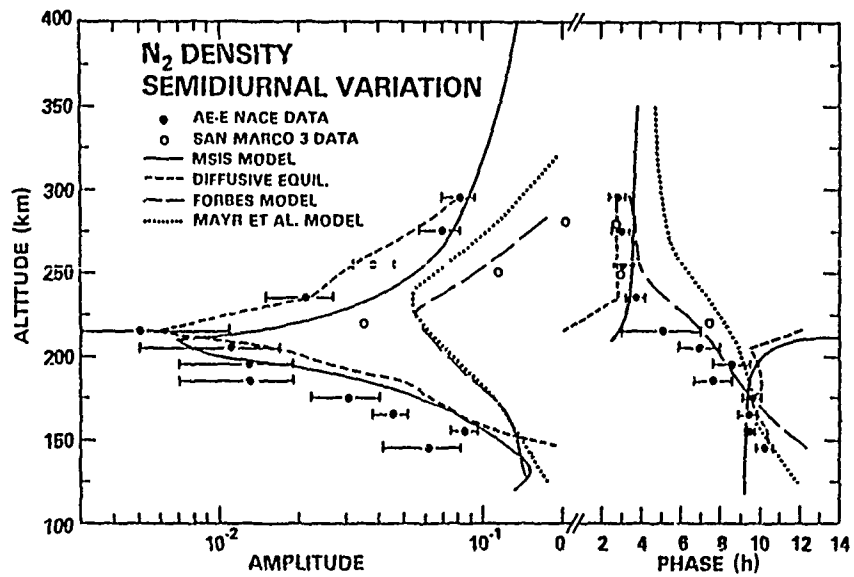


Figure 31. Molecular Nitrogen Semidiurnal Variation (Hedin et al<sup>22</sup>)

#### 4. ACCELERATION AND HEATING OF THE LOWER THERMOSPHERE DUE TO DISSIPATING TIDAL WAVES

In the zonal mean, the atmosphere can be accelerated and heated by the deposition of momentum and thermal energy by the so-called "eddy" or "perturbation" motions of the atmosphere. Since gravity wave and tidal amplitudes grow exponentially with height, it has often been suggested that these motions might contribute significantly to the mean momentum and energy budget of the lower thermosphere. These effects enter in the zonal mean momentum equation as a divergence of the eastward eddy momentum flux:

$$\bar{F}_u = \frac{1}{a \cos^2 \phi} \frac{\partial}{\partial \phi} (\overline{u'v'} \cos^2 \phi) - \frac{1}{p} \frac{\partial}{\partial z} p \overline{u'w'}$$

and in the thermal energy equation as a divergence of the thermal eddy momentum flux:

$$\bar{F}_T = - \frac{1}{a \cos \phi} \frac{\partial}{\partial \phi} (\overline{v'\phi'_z} \cos \phi) - \frac{1}{p} \frac{\partial}{\partial z} p \overline{w'\phi'_z} ,$$

where

- a = radius of the earth
- $\phi$  = latitude
- z = altitude
- p = pressure
- u' = perturbation westerly velocity
- v' = perturbation northerly velocity
- w' = perturbation vertical velocity
- $\phi'$  = perturbation geopotential.

Dickinson et al<sup>23</sup> have calculated the mean direct circulation of the lower thermosphere due to solar heating along; for comparison purposes their results for the mean zonal wind are illustrated in Figure 32. Miyahara<sup>24</sup> has investigated

- 
- 23. Dickinson, R. E., Ridley, E. C., and Roble, R. G. (1975) Meridional circulation in the thermosphere, J. Atmos. Sci. 32:1737-1735.
  - 24. Miyahara, S. (1978) Zonal mean winds induced by vertically propagating atmospheric tidal waves in the lower thermosphere, J. Meteor. Soc. Japan 56:86-98.

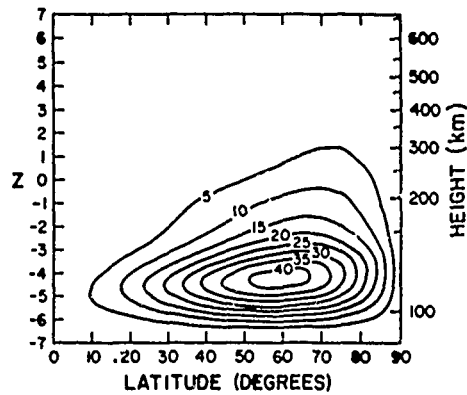


Figure 32. Mean Zonal Wind ( $\text{m sec}^{-1}$ )  
Due to Solar Heating Alone From Equinox Model of Dickinson et al<sup>23</sup>

the deposition of mean momentum and heat in the lower thermosphere connected with the dissipating (1, 1) and (2, 4) tidal modes using the above equations. In Figure 33, Miyahara's<sup>24</sup> calculation of  $F_u$  and the resulting mean zonal wind are illustrated. The (1, 1) mode is apparently capable of producing an easterly jet ( $\sim 60 \text{ m sec}^{-1}$ ) in the equatorial lower thermosphere, and a westerly flow of order  $30 \text{ m sec}^{-1}$  at midlatitudes. Results for the (2, 4) mode in Figure 34 indicate mean zonal winds of order  $10\text{-}15 \text{ m sec}^{-1}$ , which are smaller but not negligible compared with the (1, 1) mode. Note that the zonal flow generated by the dissipating tidal modes is comparable to the flow generated by direct solar heating, as illustrated in Figure 32.

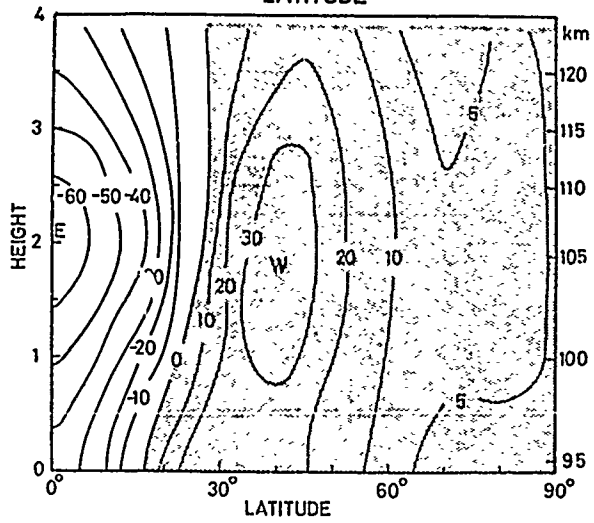
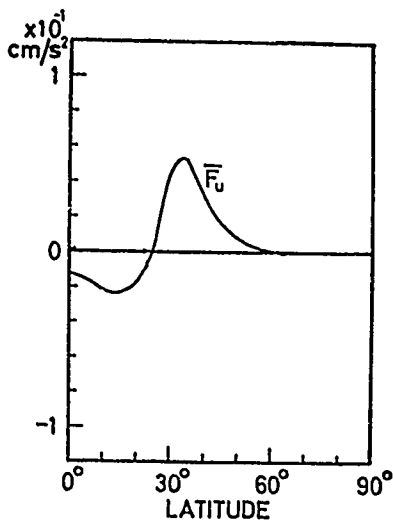


Figure 33. Divergence of Eddy Momentum Flux ( $\overline{F}_u$ ) and Zonal Mean Wind Due to (1, 1) Tidal Mode (Miyahara<sup>24</sup>)

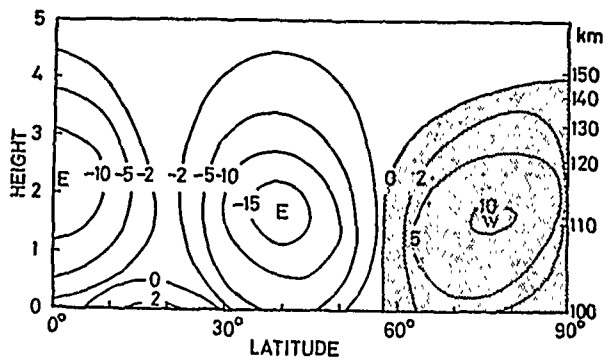
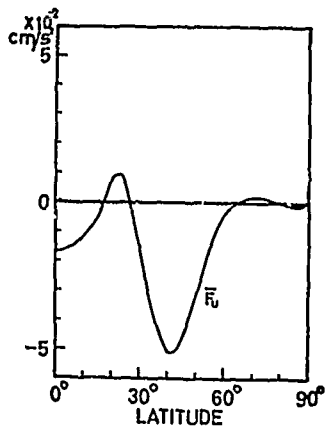


Figure 34. Divergence of Eddy Momentum Flux ( $\overline{F_u}$ ) and Zonal Mean Wind Due to (2, 4) Mode

## References

1. Forbes, J.M. (1982) Atmospheric tides. I. Model description and results for the solar diurnal component, J. Geophys. Res. 87:5222-5240.
2. Forbes, J.M. (1982) Atmospheric tides. II. The solar and lunar semi-diurnal components, J. Geophys. Res. 87:5241-5252.
3. Oliver, W. L. (1980) Improved Millstone Hill exospheric temperature measurements: evidence for a seasonal variation of the magnetic activity effect, J. Geophys. Res. 85:4237-4247.
4. Torr, M. R., Richards, R.G., and Torr, D.G. (1980) A new determination of the ultra-violet heating efficiency of the thermosphere, J. Geophys. Res. 85:6819-6826.
5. Harper, R.M. (1981) Some results on mean tidal structure and day-to-day variability over Arecibo, J. Atmos. Terr. Phys. 43:255-262.
6. Dickinson, R.E., Ridley, E.C., and Roble, R.G. (1981) A three-dimensional general circulation of model of the thermosphere, J. Geophys. Res. 86:1499-1512.
7. Mayr, H.G., Harris, I., Spencer, N.W., Hedin, A.E., Whart<sup>n</sup> L. E., Porter, H.S., Walker, J.C.G., and Carlson, H.C. (1979) Atmospheric tides and the midnight temperature anomaly, Geophys. Res. Lett. 6:447-450.
8. Lindzen, R.S., Hong, S., and Forbes, J.M. (1977) Semidiurnal Hough mode extensions into the thermosphere and their application, NRL Memorandum Rept. 3442, Naval Research Laboratory, Washington, D.C.
9. Roble, R.G. (1982) Private communication.
10. Evans, J. V. (1978) A note on lunar tides in the ionosphere, J. Geophys. Res. 83:1647-1652.
11. Hagan, M.E., Forbes, J.M., Satyanarayana, P., and Oliver, W. (1982) Exospheric temperatures at Millstone Hill: An interim analysis (in preparation).

12. Roble, R.G., Dickinson, R.E., and Ridley, E.C. (1977) Seasonal and solar cycle variations of the zonal mean circulation in the thermosphere, J. Geophys. Res. 82:5493-5504.
13. Hedin, A.E., Salah, J.E., Evans, J.V., Reber, C.A., Newton, G.P., Spencer, N.W., Kayser, D.C., Alcayde, D., Bauer, P., Cogger, L., and McClure, J.P. (1977a) A global thermospheric model based on mass spectrometer and incoherent scatter data, MSIS 1. N<sub>2</sub> density and temperature, J. Geophys. Res. 82:2139-2156.
14. Hedin, A.E., Reber, C.A., Newton, G.P., Spencer, N.W., Brinton, H.C., Mayer, H.G., and Potter, W.E. (1977b) A global thermospheric model based on mass spectrometer and incoherent scatter data, MSIS 2. Composition, J. Geophys. Res. 82:2148-2156.
15. Mayr, H.G., and Harris, I. (1977) Diurnal variations in the thermosphere -2. Temperature, composition, winds, J. Geophys. Res. 82:2628-2640.
16. Forbes, J.M. (1978) Tidal variations in thermospheric O, O<sub>2</sub>, N<sub>2</sub>, Ar, He, and H, J. Geophys. Res. 83:3691-3698.
17. Forbes, J.M., and Garrett, H.B. (1976) Solar diurnal tide in the thermosphere. J. Atmos. Sci. 33:2226-2241.
18. Forbes, J.M., and Marcos, F.A. (1980) Seasonal-latitude tidal structures of O, N<sub>2</sub> and total mass density in the thermosphere, J. Geophys. Res. 84:3489-3493.
19. Jacchia, L.G. (1977) Thermospheric Temperature, Density, and Composition: New Models, SAO Special Report 375.
20. Hedin, A.E., Spencer, N.W., Mayer, H.G., Harris, I., and Porter, H.S. (1978) Direct evidence of transport processes in thermospheric diurnal tide, J. Geophys. Res. 83:3355-3357.
21. Forbes, J.M., and Marcos, F.A. (1979) Tidal variations in total mass density as derived from the AE-E MESA experiment, J. Geophys. Res. 84:31-35.
22. Hedin, A.E., Spencer, N.W., and Mayr, H.G. (1980) The semidiurnal and terdiurnal tides in the equatorial thermosphere from AE-E measurements, J. Geophys. Res. 85:1787-1791.
23. Dickinson, R.E., Ridley, E.C., and Roble, R.G. (1975) Meridional circulation in the thermosphere, J. Atmos. Sci. 32:1737-1753.
24. Miyahara, S. (1978) Zonal mean winds induced by vertically propagating atmospheric tidal waves in the lower thermosphere, J. Meteor. Soc. Japan 56:86-98.